NATIONAL ADVISORY COMMITTEE FOR AERONAUTICS
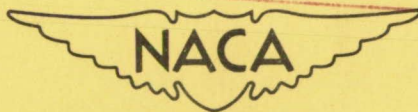
TECHNICAL NOTE 2855

GENERAL CORRELATION OF TEMPERATURE PROFILES

DOWNSTREAM OF A HEATED AIR JET DIRECTED AT

VARIOUS ANGLES TO AIR STREAM

By Robert S. Ruggeri

Lewis Flight Propulsion Laboratory
Cleveland, Ohio

NACA

Washington
December 1952

NATIONAL ADVISORY COMMITTEE FOR AERONAUTICS

TECHNICAL NOTE 2855

GENERAL CORRELATION OF TEMPERATURE PROFILES DOWNSTREAM OF A HEATED

AIR JET DIRECTED AT VARIOUS ANGLES TO AIR STREAM

By Robert S. Ruggeri

SUMMARY

An experimental investigation was conducted to determine the temperature profiles downstream of heated air jets directed at angles of 90°, 60°, 45°, and 30° to an air stream. The profiles were determined at two positions downstream of the jet as a function of jet diameter, jet density, jet velocity, free-stream density, free-stream velocity, jet total temperature, orifice flow coefficient, and jet angle. A method is presented which yields a good approximation of the temperature profile in terms of the flow and geometric conditions.

INTRODUCTION

The discharging of heated high-velocity jets of air or vapor into an air stream is employed in many installations either as a means of heating the air stream or as a method of disposing of hot discharge gases. For practical application, however, the discharging of heated jets into an air stream requires knowledge of the temperature profiles downstream of the heated jet and of the depth of penetration of the jet into the air stream.

Heating an air stream by means of heated air jets directed perpendicularly to the air stream has been previously reported in references 1 and 2. A method is presented in reference 1 by which the temperature profile and the depth of penetration of a circular heated air jet directed perpendicularly to the air stream may be predicted at any point downstream of the jet.

Because many installations employ jets which are directed at an angle other than 90° to the air stream, a study of the temperature profiles downstream of circular heated air jets directed at various angles to the air stream was conducted in the 2- by 20-inch tunnel at the NACA Lewis laboratory. Sixteen heated air jets were investigated for a range

of free-stream velocities, jet total temperatures, jet total pressures, and jet angles. The 16 jets investigated comprised a group of basic jets with four diameters and each diameter was investigated for four jet angles.

APPARATUS AND PROCEDURE

A sketch showing the experimental arrangement used in the investigation to determine the temperature profile downstream of a heated air jet issuing at various angles to an air stream is shown in figure 1(a). Heated air for the jets was obtained by passing high-pressure air through electric heaters and into a plenum chamber, the upper portion of which contained the orifice blocks. The rate of jet-air flow was measured by means of calibrated orifices located upstream of the electric heaters. Each of the 16 jet orifices was investigated for a range of jet pressure ratios (ratio of jet total pressure measured at exit to outlet static pressure) from 1.2 to 3.5. The jet total pressure was measured by means of a pressure tap located in the wall of the plenum chamber and was corrected for total pressure loss through the flow passages. (Bench tests were conducted to determine the pressure loss through the passages under choked-flow condition in still air.) The jet total temperatures and free-stream velocities investigated were nearly constant values of 660° and 860° F, and 235 and 400 feet per second, respectively. The temperature profiles were measured by means of a movable thermocouple rake which consisted of 33 thermocouple probes spaced 0.250 inch apart. The thermocouple rake was inserted at positions 6.47 and 18.0 inches downstream of the discharge-orifice center.

The orifices used in the investigation consisted of smooth circular holes machined in cast Inconel orifice blocks as shown in figure 1(b). The orifice holes were 0.250, 0.375, 0.500, and 0.625 inch in diameter and each orifice was investigated at jet angles β of 90°, 60°, 45°, and 30° to the air stream. Although the holes are circular in cross section, the plan form of the orifices (jet exit) is elliptical in a plane parallel to the main stream except for the cases where the jet angle β is 90°. The orifice blocks were so machined that the center line of the 16 orifices investigated passed through the same point at the surface of the model. The length of the passage through the various orifice blocks varied in length from 2.0 inches for jets issuing at 90° to the air stream to 4.0 inches for the jets discharging at 30° to the main tunnel flow. The term "orifice diameter" or "jet diameter" is used throughout this report when referring to the diameter of the discharge opening measured perpendicular to the jet axis (fig. 1(b)).

The tunnel boundary layer was removed by suction upstream of the orifices to minimize tunnel wall boundary-layer effects (see fig. 1).

SYMBOLS

The following symbols are used in this report:

a, b, g, h, i, k exponents for correlating depth of jet penetration into air stream X_1

d, e, f exponents for correlating X_2 (see fig. 2)

C discharge-orifice flow coefficient, dimensionless

D_j diameter of discharge orifice, in.

M_L slope of lower portion of temperature profile curve, in./$^{\circ}$F

M_U slope of upper portion of temperature profile curve, in./$^{\circ}$F

s mixing distance or distance measured downstream of center of discharge orifice to plane of temperature survey, in.

T_j total temperature of jet, $^{\circ}$R

T_0 total temperature of free stream, $^{\circ}$R

ΔT total-temperature rise above free-stream total temperature measured at any distance X normal to model surface for given temperature profile, $^{\circ}$F

ΔT_m maximum total-temperature rise above free-stream total temperature, $^{\circ}$F

ΔT_1 temperature minimum measured on lower portion of temperature profile, $^{\circ}$F (see fig. 2(d))

V_j velocity of jet at exit, ft/sec

V_0 velocity of free stream, ft/sec

w width of jet boundary at any distance s downstream of center of discharge orifice, in.

X distance normal to model surface, in.

X_1 depth of jet penetration into air stream as determined by intersection of line of slope M_U with value of $\Delta T = 0$, in.

X_2 value of X as determined by intersection of line of slope M_L with value of $\Delta T = \Delta T_M$, in.

β angle with tunnel air flow at which jet discharges into air stream, deg

θ_L arc tan of M_L

θ_U arc tan of M_U

μ_j viscosity of jet at exit, slugs/ft-sec

μ_0 viscosity of free stream, slugs/ft-sec

ρ_j mass density of jet at exit, slugs/cu ft

ρ_0 mass density of free stream, slugs/cu ft

$\varphi_1 \cdot \cdot \cdot \varphi_5$ correlation parameters

ANALYSIS

The purpose of the analysis presented herein is to obtain a method by which the temperature profile downstream of a heated air jet directed at various angles to an air stream may be predicted, if the flow and geometric conditions are known.

The results of an earlier investigation (reference 1) indicate that the approximate temperature profile downstream of a heated air jet directed perpendicularly to an air stream may be calculated by use of dimensionless parameters. The present investigation was undertaken to extend the results of this earlier experiment to include jets discharging at various angles to the air stream. In reference 1, the penetration coefficients $X_1/\sqrt{C}\ D_j$ and $X_2/\sqrt{C}\ D_j$, the upper and lower slope coefficients $M_U(T_j-T_0)/D_j$ and $M_L(T_j-T_0)/D_j$, and the maximum temperature rise coefficient $\Delta T_m w/C D_j (T_j-T_0)$ were correlated in terms of the density ratio ρ_j/ρ_0, velocity ratio V_j/V_0, mixing distance to diameter

ratio s/D_j, and width coefficient w/D_j. The parameters are in most cases self-explanatory; however, the width coefficient w/D_j may be used in two significantly different ways depending on whether or not the jet under consideration is discharging as a free (unrestricted) or as a confined (restricted) jet. The symbol w in the width coefficient is defined as the width, or amount of expansion, of the jet measured at any distance s downstream of the discharge orifice; hence, for the case of a free jet, the value of the width coefficient increases continuously with increasing values of mixing distance. If the jet is confined (as in references 1 and 2 and herein), the width coefficient increases with increasing mixing distance, until at some distance s downstream of the discharge orifice, the jet has expanded sufficiently to contact the tunnel walls (see fig. 1(c)). At this point, the width coefficient has attained its maximum value for a given discharge-orifice diameter and remains constant for further increases in mixing distance. A further discussion on the proper use of the width coefficient is presented in the section EXTRAPOLATION OF RESULTS TO WIDER RANGE OF VARIABLES. The results presented in reference 1 indicate that the use of the effective discharge-orifice diameter $\sqrt{C} \, D_j$ and the ratio $s/\sqrt{C} \, D_j$, in place of the actual discharge-orifice diameter D_j and the ratio s/D_j, generalized the data and resulted in better correlation. This substitution also yielded a better correlation of the data obtained for this investigation and was used wherever the method of analysis permitted. In order to differentiate between the ratios $s/\sqrt{C}D_j$ and s/D_j, the term s/D_j is defined as the ratio of mixing distance to diameter ratio and $s/\sqrt{C}D_j$ is defined as the ratio of mixing distance to effective diameter.

In an over-all study of the profile data for jets discharging at an angle of 90° to the air stream, certain consistent characteristics of the profiles were observed which suggested a simplified means for correlating the data. These characteristics were noted in a study of the profiles at jet pressure ratios greater than choking for a particular orifice diameter, mixing distance, free-stream velocity, and jet total temperature. A typical example of the type of temperature profile measured downstream of a jet discharging at right angles to the air stream is shown in figure 2(a). It was noted in the study that for a given discharge-orifice diameter, jet total temperature, free-stream velocity, and mixing distance, the upper and lower slopes, M_U and M_L, approximated linear segments which remained parallel for jet pressure ratios greater than the choking value of 1.87. Also, it was found that the maximum temperature rise ΔT_m decreased slightly with decreasing jet pressure ratio. A study of the temperature profiles for other orifice diameters, mixing distances, and free-stream velocities showed the same characteristics for pressure ratios greater than choking. The temperature profiles measured downstream of a jet

discharging at an angle of 90° to the air stream were therefore approx-
imated by three straight lines as shown in figure 2(a) where the dis-
tance normal to the model surface X is plotted against the total-
temperature rise above free-stream total temperature ΔT. Because the
upper and lower slopes of the profiles are independent of pressure ratio
for values greater than choking, the analysis was limited to jet pres-
sure ratios greater than 1.87.

In a study of the data for jets issuing at angles of 60°, 45°, and
30° to the air stream, it was found that in most instances, the general
shape of the temperature profiles differed greatly from that obtained
for a jet discharging at an angle of 90° (fig. 2(a)). However, the
study also showed that these various types at profile had certain con-
sistent characteristics similar to those noted for a jet discharging at
90° to the air stream. It was found that four basic types of tempera-
ture profile, measured downstream of the jets, could be used to repre-
sent the profile data for all jet diameters and jet angles investigated
(fig. 2). Also shown in figure 2 is the manner in which these profiles
are approximated by straight lines.

The depth of penetration X_1 and X_2, the upper and lower slopes
M_U and M_L, and the maximum temperature rise ΔT_m are identical to
those defined in reference 1. The term ΔT_m (type IV) is defined as
the temperature rise above free-stream temperature measured at the
temperature minimum point on the lower portion of the temperature pro-
file. Jet velocities and densities were calculated from total-pressure
and -temperature measurements by the method presented in reference 3.

The type of temperature profile obtained downstream of a particu-
lar jet is a function of the orifice diameter, the velocity ratio, the
mixing distance to diameter ratio, and the jet angle β. It was found
in certain instances that a jet of given diameter, issuing at a given
angle to the air stream, yielded as many as three types of profile for
the values of the velocity ratio and the mixing distance to diameter
ratio investigated. The transition of the temperature profiles from
one type to another was not exactly defined by the data since only two
values of mixing distance and two tunnel-air velocities were included
in the investigation. As a result, it was necessary to tabulate the
conditions at which the various types of profile were obtained. The
ranges of velocity ratio and mixing distance to diameter ratio at which
these various types of temperature profile occur are presented in
table I for various values of orifice diameter and jet angle. It can
be noted from table I that only jets which issue at right angles to the
air stream yield the same type profile (type I) for all conditions
investigated. Also, the majority of the data obtained yielded a type I
or type II temperature profile. Type III and type IV profiles occurred
only at the lowest value of mixing distance investigated (s = 6.47 in.).

The importance of table I will become evident in the discussions that follow.

RESULTS AND DISCUSSION

Flow Coefficient

The discharge-orifice flow coefficient C is defined as the ratio of the actual measured mass flow to the theoretical mass flow. The actual mass flow through the various discharge orifices was measured by means of calibrated measuring orifices located upstream of the electric heaters. The theoretical mass flow was calculated from the compressible flow relations based on conditions at the jet exit. (Bench tests were made to determine the pressure loss through the jet flow passages under choked flow conditions.) The total-temperature loss through the jet flow passages was found to have a negligible effect on the flow coefficient (less than 0.5 percent). As expected, the measured flow coefficient for all the jets investigated was found to be independent of jet pressure ratio at values greater than choking. The flow coefficient ranged from 0.88 to 0.92 for all jets investigated and the arithmetic average was 0.90. Because the measured flow coefficients obtained for the orifices used in this investigation may not be applicable for other installations, no data for the flow coefficients are presented in this report.

Correlation of Penetration Coefficient $X_1/\sqrt{C}\ D_j$

The over-all parameter obtained for correlation of the penetration coefficient $X_1/\sqrt{C}\ D_j$ for a jet issuing at right angles to the air stream $(\beta = 90^\circ)$ was found to be $\varphi_1 (\rho_j/\rho_0)^a (V_j/V_0)^b (s/\sqrt{C}\ D_j)^{0.26}$. The variation of the penetration coefficient $X_1/\sqrt{C}\ D_j$ with this over-all parameter is shown in figure 3 for all discharge-orifice diameters, mixing distances, free-stream velocities, and jet total temperatures investigated. Although this correlation curve applies for the two jet total temperatures investigated, only the data obtained for a jet total temperature of 860° R are presented. The data obtained for a jet total temperature of 660° R yielded an identical correlation curve. The linear variation of the penetration coefficient with its over-all parameter is dictated by the method of correlation used. The method employed in this investigation is identical to that presented in reference 1, and hence, no details of correlation are presented herein. The density-ratio exponent a and the velocity-ratio exponent b were found to decrease with decreasing discharge-orifice diameter, indicating

an effect of width coefficient w/D_j. The variation of these exponents with width coefficient is shown in figure 4(a). The values shown are identical to those obtained in the correlation when a thin-plate orifice was used (reference 1).

The correlation parameter φ_1 was found to increase with increasing width coefficient w/D_j and to become asymptotic to a finite value at high values of width coefficient (fig. 4(b)). A study of the figure shows that for a constant value of width coefficient, the term φ_1 decreases slightly with decreasing jet total temperature. The values of φ_1 presented in figure 4(b) are slightly lower than the corresponding values obtained with a thin-plate orifice (reference 1). The variation of φ_1 with jet total temperature actually indicates an effect of viscosity ratio μ_j/μ_0. However, for the ranges of jet and free-stream temperature investigated, the viscosity of air is proportional to a power of the absolute temperature, and hence, the viscosity ratio μ_j/μ_0 may be presented in terms of the absolute temperature ratio T_j/T_0. The exponent of the ratio of the mixing distance to effective diameter $s/\sqrt{C} \, D_j$ was found to remain constant for all diameters investigated at $\beta = 90^{\circ}$. For comparison, calculations were made using the results of reference 1 and the faired curves presented herein, and it was found that jets discharging from both short circular passages and circular thin-plate orifices yield very nearly equal depths of penetration X_1.

The over-all parameter obtained for correlation of the penetration coefficient $X_1/\sqrt{C} \, D_j$ for a jet issuing at 60° to the air stream was found to be $\varphi_2(\rho_j/\rho_0)^{0.49}(V_j/V_0)^{0.49}(s/\sqrt{C} \, D_j)^{0.25}$. The linear variation of the penetration coefficient with this parameter is shown in figure 5 for all values of orifice diameter, mixing distances, free-stream velocities, and temperature ratios investigated. The density-ratio exponent, the velocity-ratio exponent, and the ratio of mixing distance to effective diameter exponent were found to remain constant for all orifice diameters or width coefficients investigated. The variation of the correlation parameter φ_2 with width coefficient w/D_j is shown in figure 6 for constant values of temperature ratio.

The parameter obtained for correlation of the penetration coefficient $X_1/\sqrt{C} \, D_j$ for a jet issuing at an angle of 45° to the air stream was found to be $\varphi_3(\rho_j/\rho_0)^g(V_j/V_0)^h(s/\sqrt{C} \, D_j)^{0.30}$. The penetration coefficient is shown plotted as a function of this parameter in figure 7

for all conditions investigated. As was observed for the case of a jet
issuing at right angles to the air stream, the density-ratio exponent,
the velocity-ratio exponent, and the correlation parameter φ_3 were
all found to be functions of the width coefficient. The variation of
the density- and velocity-ratio exponents g and h with the width
coefficient is shown in figure 8(a). The variation of the correlation
parameter φ_3 with width coefficient is shown plotted in figure 8(b)
for constant values of temperature ratio.

The over-all parameter obtained for correlation of the penetration
coefficient $X_1/\sqrt{C} \, D_j$ for a jet issuing at an angle of 30° to the air
stream was found to be $\varphi_4 (\rho_j/\rho_0)^i (V_j/V_0)^k (s/\sqrt{C} \, D_j)^{0.36}$. The variation
of the penetration coefficient with this parameter is shown in figure 9.
The density-ratio exponent, the velocity-ratio exponent, and the corre-
lation parameter φ_4 were again found to be a function of the width
coefficient. The variation of the density-ratio exponent i and the
velocity-ratio exponent k with width coefficient is shown plotted
in figure 10(a). Figure 10(b) shows the variation of the correlation
parameter φ_4 with width coefficient.

Correlation of Penetration Coefficient $X_2/\sqrt{C} \, D_j$

A correlation of the penetration coefficient $X_2/\sqrt{C} \, D_j$ for a jet
angle of 90° yielded the following correlation parameter:

$$\varphi_5 (\rho_j/\rho_0)^d (V_j/V_0)^e \left(\frac{s}{\sqrt{C} \, D_j}\right)^{-f}$$

The variation of the penetration coefficient with this ·correlation
parameter is plotted in figure 11.

The velocity-ratio exponent e, the ratio of the mixing distance
to effective diameter exponent f, and the correlation parameter φ_5
were all found to be functions of the width coefficient, whereas the
density-ratio exponent d was found to be a function of the mixing
distance to diameter ratio s/D_j. The curves showing the variation of
the exponents d, e, f, and φ_5 with their respective parameters are
shown in figures 12 and 13. The values obtained for exponents d, e,
and f were found to be identical to those reported in reference 1.
As can be noted in figure 13(b), the values of φ_5 varied slightly
from the corresponding values presented in reference 1.

The over-all parameter obtained for correlation of the penetration coefficient $X_2/\sqrt{C} \ D_j$ for a jet issuing at an angle of 60° was found to be

$$(\rho_j/\rho_0)^{0.53} (V_j/V_0)^{0.60} (s/\sqrt{C} \ D_j)^{0.75}$$

The penetration coefficient is shown plotted as a function of the correlation parameter in figure 14 for constant values of temperature ratio. In the analysis of the penentration (X_2) data for jets discharging at 60°, 45°, and 30° to the air stream, it was found that the correlation parameter φ was independent of the width coefficient for a given jet total temperature. Because the jets were investigated for only two values of jet total temperature, the term φ has only two values for a given jet angle β and therefore was not included in the correlation. The exclusion of the term φ from the parameter results in the separated curves presented in figure 14. In addition, no data are shown plotted in figure 14 for the 0.625-inch-diameter orifice. This results from the fact that for all conditions investigated, the 0.625-inch-diameter jet yielded only type II and type III profiles for which no value for X_2 exists (see table I).

The parameters obtained for the final correlation of the penetration coefficient $X_2/\sqrt{C} \ D_j$ for jets issuing at 45° and 30° to the air stream were found to be

$$(\rho_j/\rho_0)^{0.62} (V_j/V_0)^{0.71} (s/\sqrt{C} \ D_j)^{0.60}$$

and

$$(\rho_j/\rho_0)(V_j/V_0)^{0.71} (s/\sqrt{C} \ D_j)^{0.60}$$

respectively. The variation of the penetration coefficients with these parameters is presented in figures 15 and 16 for constant values of temperature ratio. Much of the scatter in figures 11, 14, 15, and 16 results from the difficulty in determining X_2 from the temperature profiles. In most instances, the values of X_2 are so small that a small difference in reading the temperature and fairing the profiles resulted in errors of as much as 20 percent in X_2. Although these errors are rather large percentagewise, the actual error in the over-all profile should not preclude its practical usefulness.

Correlation of Slope Coefficients

In previous discussion of the profile characteristics, it was noted that the upper and lower slopes of the profiles were independent of jet pressure ratio for pressure ratios greater than 1.87. The slopes are therefore independent of density ratio and its effect need not be considered in this analysis. In addition, because the jets are choked, the jet velocity is constant for a particular value of jet total temperature, and hence the velocity ratio is constant for a particular value of free-stream velocity. For all the data obtained over a range of jet pressure ratios for a given value of mixing distance, jet diameter, jet angle, jet total temperature, and free-stream velocity, the slope may therefore be represented by a single value. Proceeding with the analysis from this point yielded the parameters for correlation of the upper and lower slope coefficients. The upper and lower slope coefficients are defined as $M_U(T_j-T_0)/D_j$ and $M_L(T_j-T_0)/D_j$, respectively.

Upper slope coefficient. - The parameter obtained for correlation of the upper slope coefficient for a jet angle of 90° was found to be

$$(V_j/V_0)^{0.65}(s/D_j)^{0.91}(w/D_j)$$

which resulted in a linear variation as shown in figure 17. This parameter is identical to that reported in reference 1 with the exception that the mixing distance to diameter ratio exponent was found to be slightly lower (0.91) than that previously obtained (1.0) for a jet issuing from a thin-plate orifice.

For the case of a jet issuing at an angle of 60° to the air stream, the parameter obtained for correlation was found to be $(V_j/V_0)^{0.57}(s/D_j)^{1.06}(w/D_j)^{0.63}$. The upper slope coefficient $M_U(T_j-T_0)/D_j$ is shown plotted as a function of this parameter in figure 18.

The final parameter obtained for correlation of the upper slope coefficient for a jet issuing at an angle of 45° to the air stream was found to be $(V_j/V_0)^{0.51}(s/D_j)^{1.18}(w/D_j)^{0.43}$, as shown in figure 19.

The parameter obtained for correlation of the upper slope coefficient for a jet issuing at an angle of 30° to the air stream was found to be $(V_j/V_0)^{0.44}(s/D_j)^{1.39}(w/D_j)^{0.24}$, as shown in figure 20.

A comparison of figures 17 through 20 shows that the velocity-ratio exponent and the width-coefficient exponent increase with increasing jet angle. The mixing distance to diameter ratio exponent decreases with increasing jet angle.

Lower slope coefficient. - The correlation of the lower slope coefficient $M_L(T_j-T_0)/D_j$ for jets issuing at an angle of 90° to the air stream yielded a parameter identical to that reported in reference 1. Figure 21 shows the linear variation of the lower slope coefficient with the parameter $(s/D_j)^{1.25}(V_j/V_0)^{0.53}$ for various values of jet total temperature.

Jets issuing at an angle of 60° to the air stream yield type II, III, and IV temperature profiles. Of these types, only the type IV profile yields a measurable lower slope. The lower slopes of the type II profile appear as vertical straight lines (infinite slope), and from the method of approximation employed, the negative values of the lower slope for the type III profile were neglected. Therefore, for jets issuing at an angle of 60°, only the lower slopes of the type IV profile were considered. The final correlation of the lower slope coefficient for $\beta = 60^O$ is shown plotted in figure 22 as a function of mixing distance to diameter ratio for various values of velocity ratio. The area between the dashed lines indicates the range of mixing distance to diameter ratio over which a value of lower slope was obtained.

In analyzing the data for jets issuing at an angle of 45° to the air stream, the lower slope coefficient was again found to be a function of the mixing distance to diameter ratio. The variation of the lower slope coefficient with the mixing distance to diameter ratio is shown plotted in figure 23 for various values of width coefficient. The solid curve indicates that only the 0.250-inch-diameter jet yielded temperature profiles with a measurable lower slope for both values of mixing distance investigated. The dashed lines indicate that the jets with diameters of 0.625, 0.500, and 0.375 inch yielded profiles with measurable lower slopes only for the lower values of mixing distance to diameter ratio investigated (corresponding to s = 6.47 inches). For the higher values of mixing distance to diameter ratio (corresponding to s = 18.0 inches), these jets yielded type II temperature profiles which have an infinite lower slope. The dashed lines therefore extend to infinity at the values of s/D_j presented in the figure, and although these lines are probably not highly accurate, they do show the general trend of the data. It was not possible to determine the value of mixing distance to diameter ratio at which the profiles changed from one type to another.

NACA TN 2855   13

An analysis of the lower slope coefficients for jets issuing at an angle of $30°$ resulted in a correlation very similar to that previously described for $\beta = 45°$. A plot showing the variation of the lower slope coefficient with mixing distance to diameter ratio for various values of width coefficient is shown in figure 24.

Correlation of Maximum Temperature-Rise Coefficient

The maximum temperature-rise coefficient presented in reference 1 is $\Delta T_m w / C(T_j - T_0) D_j$ and includes the orifice-flow coefficient C. In reference 1 the maximum temperature rise ΔT_m was found to decrease slightly with decreasing jet pressure ratio. The flow coefficient for thin-plate orifices also decreased with decreasing pressure ratio (reference 3); hence, the ratio $\Delta T_m / C$ was investigated and found to be independent of pressure ratio. Therefore, for a given value of orifice diameter, mixing distance, free-stream velocity, and jet total temperature, the term $\Delta T_m / C$ was a constant for all values of jet pressure ratios investigated greater than choking. Further investigation showed that for a given set of conditions, the maximum temperature rise was also independent of the velocity ratio V_j / V_0. An increase in free-stream velocity and a consequent decrease in penetration varied the profile such that the maximum temperature rise ΔT_m remained constant. Because the term $\Delta T_m / C$ was found to be independent of both the density (pressure) and velocity ratios, it was possible to construct a plot of $\Delta T_m / C$ against the mixing distance to diameter ratio s/D_j. The effect of jet total temperature on maximum temperature rise was then taken into account by the introduction of the temperature difference $(T_j - T_0)$ into the coefficient. A plot of $\Delta T_m / C(T_j - T_0)$ against s/D_j yielded four curves where each curve represented a constant value of width coefficient. When the width coefficient was included in the correlation, a single curve and the maximum temperature-rise coefficient $\Delta T_m w / C(T_j - T_0) D_j$ mentioned previously and reported in reference 1 was obtained.

In this investigation, the maximum temperature rise was also found to be independent of the velocity ratio and to decrease slightly with decreasing jet pressure ratio. However, the flow coefficient was found to be nearly constant for all conditions investigated and thus was not included in the correlation. It was therefore necessary to begin the correlation with the temperature-rise parameter $\Delta T_m / (T_j - T_0)$ and to proceed with the correlation in the same manner as that reported in reference 1 until a correlation parameter was obtained. For jets issuing at an angle of $90°$ to the air stream, this resulted in a correlation, as shown in figure 25, where the temperature-rise coefficient $\Delta T_m w / D_j (T_j - T_0)$ is shown plotted as a function of mixing

distance to diameter ratio. The data presented in reference 1 were
recalculated using this new temperature-rise coefficient, and for com-
parison, the faired curve representing these results was also plotted
in figure 25. No additional scatter was evident due to the slight
change in the correlation. From the comparison shown in figure 25, the
maximum temperature rise obtained using a 2-inch passage is very nearly
the same as that obtained using a thin-plate orifice. Although the
variation of maximum temperature rise with jet pressure ratio has not
been taken into account, this variation is small (of the order of 3° to
5° F) and within the over-all accuracy of the other coefficients pre-
sented in this report.

An analysis of the data for a jet issuing at an angle of 60°
resulted in the maximum temperature-rise coefficient
$\Delta T_m(w/D_j)^{1.48}/(T_j-T_0)$. The variation of this coefficient with mixing
distance to diameter ratio is shown plotted in figure 26 for the var-
ious orifice diameters investigated.

The final maximum temperature-rise coefficient for jets issuing
an angle of 45° to the air stream was found to be $\Delta T_m(w/D_j)^{1.18}/(T_j-T_0)$
and is shown plotted in figure 27 as a function of the mixing distance
to diameter ratio. A study of figures 26 and 27 shows that the maximum
temperature-rise coefficient remains constant for small values of mix-
ing distance to diameter ratio.

An analysis of the data for a jet issuing at an angle of 30°
resulted in the maximum temperature-rise coefficient
$\Delta T_m(w/D_j)^{0.64}/(T_j-T_0)$. This coefficient is shown plotted in figure 28
as a function of the mixing distance to diameter ratio s/D_j.

Calculations using the faired curves from figures 25 to 28 show
that for values of the mixing distance to diameter ratio greater than
approximately 70, the maximum temperature rise becomes nearly inde-
pendent of the jet angle. For lower values of s/D_j, the maximum tem-
perature rise increases with decreasing jet angle.

Correlation of Temperature Rise Coefficient $\Delta T_1/(T_j-T_0)$

From figure 2 it was noted that the type IV profile has a temper-
ature minimum point on the lower portion of the temperature profile.
The total-temperature rise above free-stream total temperature measured
at this minimum point is ΔT_1, and the term $\Delta T_1/(T_j-T_0)$ is defined
as the temperature-rise coefficient. In order to better approximate
the measured profile, a correlation of the temperature-rise coeffi-
cient was made and the coefficient was found to be a function of the

mixing distance to diameter ratio for all flow and geometric conditions which yield a type IV profile. Figure 29 shows the variation of the temperature-rise coefficient $\Delta T_1/(T_j-T_0)$ with the mixing distance to diameter ratio for jet angles of 60°, 45°, and 30°. These curves are applicable only for the conditions listed in table I.

Comparison of Calculated and Experimental Profiles

The correlation of the various coefficients with the flow and geometric parameters presented in the foregoing discussion provides a method by which an approximation of the temperature profile downstream of a heated-air jet directed at an angle to the air stream may be obtained.

Based on the experimental conditions, a number of profiles were calculated and compared with the actual profiles. Some typical examples are shown in figure 30. A study of this figure shows that, in general, the approximate solution is in good agreement with the experimental data and provides a reasonably simple method for obtaining the temperature profile downstream of a heated-air jet directed at an angle to the air stream.

Although the results presented in this report are for pressure ratios greater than the choking value of 1.87 (based on exit conditions), the investigation included data at pressure ratios below choking. These data are not shown in the curves because of the method of correlation employed. An analysis of the limited amount of data obtained at jet pressure ratios below choking has shown that the various types of temperature profiles have a strong tendency to change to type I profiles for small values of pressure ratio. In an analysis of data obtained for jets which yield type I profiles, it was found that by using the method presented herein, reasonably good agreement was obtained between the experimental and calculated profiles for a range of jet pressure ratios from 1.2 to 1.87 (a typical example is shown in fig. 31). For jets issuing at angles which yield other than type I profiles, calculations showed that the penetration X_1, the upper slope M_U, and the maximum temperature rise ΔT_m are in good agreement with the measured profile. The data presented herein are for jet pressure ratios greater than the choking value of 1.87, and since no lower slope exists for the type II and type III profiles at these high pressure ratios, the lower portion of the type II and III profiles cannot be predicted for jet pressure ratios less than choking by the method presented herein.

Because boundary-layer removal was employed throughout the investigation, the effect of boundary-layer thickness on the temperature profile was not determined.

EXTRAPOLATION OF RESULTS TO WIDER RANGE OF VARIABLES

The usefulness of the correlations previously given is restricted primarily by the range of variables. The greatest restriction in the method proposed is the limited range of width coefficient investigated. The expansion of the jets downstream of the jet exit was confined by the tunnel walls, and hence the maximum value of width coefficient obtained for each diameter orifice investigated was limited by the physical dimensions of the tunnel. However, if the width of a jet (whether restricted or unrestricted) can be predicted at any point downstream of the jet exit, it should be possible to utilize the results presented herein over a greater range of variables and obtain reasonably good results.

No data are available on the spreading (expansion) characteristics of jets directed at angles to the air stream; however, there are some data on the spreading characteristics of jets directed parallel to an air stream. Because a jet directed at an angle to the air stream is turned very rapidly by the air stream, the expansion probably closely approximates that of a jet directed parallel to the air stream. If this assumption is made, the spreading characteristics of a free jet directed at an angle to the air stream can be calculated by the method presented in reference 4. The results of reference 4 are based on the turbulent mixing of an incompressible fluid and yield the momentum rather than the thermal jet width. The thermal jet width can be obtained from turbulent-mass and heat-exchange considerations, wherein the ratio of thermal width to momentum width has been found to equal $\sqrt{2}$ (reference 5). The thermal expansion of a free jet, calculated on this basis, is shown in figure 32. The jet-width coefficient w/D_j is shown plotted as a function of the mixing distance to diameter ratio for several values of the velocity ratio.

Before calculating the various parameters needed for obtaining the temperature profiles, it is necessary to first determine the proper jet-width coefficient at the mixing distance in question. If, for the problem being considered, the jet is discharging into an unbounded air stream, the jet is unrestricted and the width coefficient has but one possible value for a given s/D_j (fig. 32). If the jet being considered is discharging into a duct, the proper width coefficient to use in calculations is dependent on whether or not the jet is restricted. If the jet-width coefficient as determined from figure 32 is greater than the duct-width coefficient, the jet is restricted in its expansion

and the duct-width coefficient is the important parameter. If the jet-width coefficient is less than the duct-width coefficient, the jet is relatively unrestricted and the jet-width coefficient becomes the important parameter and should be used in the calculations.

COMPARISON OF CALCULATED AND EXPERIMENTAL JET BOUNDARIES

During the course of the investigation, numerous photographs of the jet boundary were made by means of the schlieren technique and the results were compared with the calculated jet boundary obtained by use of the correlation curves presented herein. For illustrative purposes, the calculated boundaries were obtained from both a constant value of width coefficient based on tunnel dimensions and a variable jet-width coefficient based on the actual width of the jet at the point of interest (fig. 32). Some typical examples of the comparisons obtained are shown in figure 33 for the four jet angles investigated. The distance normal to the model surface is shown plotted against the mixing distance. A study of this figure shows that use of the width coefficient based on the actual jet width yields calculated profiles which are in reasonably good agreement with the measured profile obtained from schlieren photographs. The use of a constant width coefficient, based on tunnel dimensions, yields calculated profiles which deviate considerably from the actual profile for small values of mixing distance where the jet is not confined by the tunnel walls. The value of mixing distance at which the two calculated curves become one curve is the point beyond which the jet becomes confined by the walls of the tunnel.

A study of the schlieren photographs also shows that the lower jet boundary leaves the surface of the model before sufficient expansion and mixing of the jet with the air stream takes place to enable the jet to contact the surface. The surface distance downstream of the orifice which is unheated by the jet increases with decreasing jet angle for the range of jet angle investigated.

CONCLUDING REMARKS

A method which provides a reasonably simple means of obtaining the approximate temperature profile downstream of a heated-air jet directed at an angle to the air stream has been presented in terms of dimensionless parameters of the flow and geometric conditions.
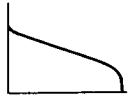
Lewis Flight Propulsion Laboratory
    National Advisory Committee for Aeronautics
        Cleveland, Ohio

REFERENCES

1. Callaghan, Edmund E., and Ruggeri, Robert S.: A General Correlation
     of Temperature Profiles Downstream of a Heated-Air Jet Directed
     Perpendicularly to an Airstream. NACA TN 2466, 1951.

2. Ruggeri, Robert S., Callaghan, Edmund E., and Bowden, Dean T.: Pene-
     tration of Air Jets Issuing from Circular, Square, and Elliptical
     Orifices Directed Perpendicularly to an Airstream. NACA TN 2019,
     1950.

3. Callaghan, Edmund E., and Bowden, Dean T.: Investigation of Flow
     Coefficient in Circular, Square, and Elliptical Orifices at High
     Pressure Ratios. NACA TN 1947, 1949.

4. Squire, H. B., and Trouncer, J.: Round Jets in a General Stream.
     Rep. No. Aero. 1904, British R.A.E., Jan. 1944.

5. Szablewski, W.: The Diffusion of a Hot Air Jet in Air in Motion.
     NACA TM 1288, 1950.

TABLE I - CONDITIONS AT WHICH VARIOUS TYPES OF TEMPERATURE PROFILE WERE OBTAINED

Profile type	Jet angle β (deg)	Orifice diameter D_j (in.)	Free-stream velocity V_0 (ft/sec)	Mixing distance to diameter ratio range s/D_j	Mixing distance s (in.)	Velocity ratio range V_j/V_0
I	90	0.625, 0.500, 0.375, 0.250	235 and 400	10.4-72.0	6.47 and 18.0	2.9-3.3; 4.9-5.7
	60	---	---	---	---	---
	45	0.625, 0.500, 0.375, 0.250	400	10.4-25.9	6.47	2.9-3.3
	45	0.250	235 and 400	72.0	18.0	4.9-5.7
	30	0.625, 0.500, 0.375, 0.250	400	10.4-25.9	6.47	2.9-3.3
	30	0.250	235 and 400	72.0	18.0	4.9-5.7
II	90	---	---	---	---	---
	60	0.625, 0.500, 0.375, 0.250	235 and 400	28.8-72.0	18.0	2.9-3.3; 4.9-5.7
	45	0.625, 0.500, 0.375	235 and 400	28.8-48.0	18.0	2.9-3.3; 4.9-5.7
	30	0.625, 0.500, 0.375	235 and 400	28.8-48.0	18.0	2.9-3.3; 4.9-5.7
III	90	---	---	---	---	---
	60	0.625 / 0.500	235 and 400 / 235	10.4 / 12.9	6.47 / 6.47	2.9-3.3; 4.9-5.7 / 4.9-5.7
	45	---	---	---	---	---
	30	---	---	---	---	---
IV	90	---	---	---	---	---
	60	0.500 / 0.375, 0.250	400 / 235 and 400	12.9 / 17.2-25.9	6.47 / 6.47	2.9-3.3 / 2.9-3.3; 4.9-5.7
	45	0.625, 0.500, 0.375, 0.250	235	10.4-25.9	6.47	4.9-5.7
	30	0.625, 0.500, 0.375, 0.250	235	10.4-25.9	6.47	4.9-5.7
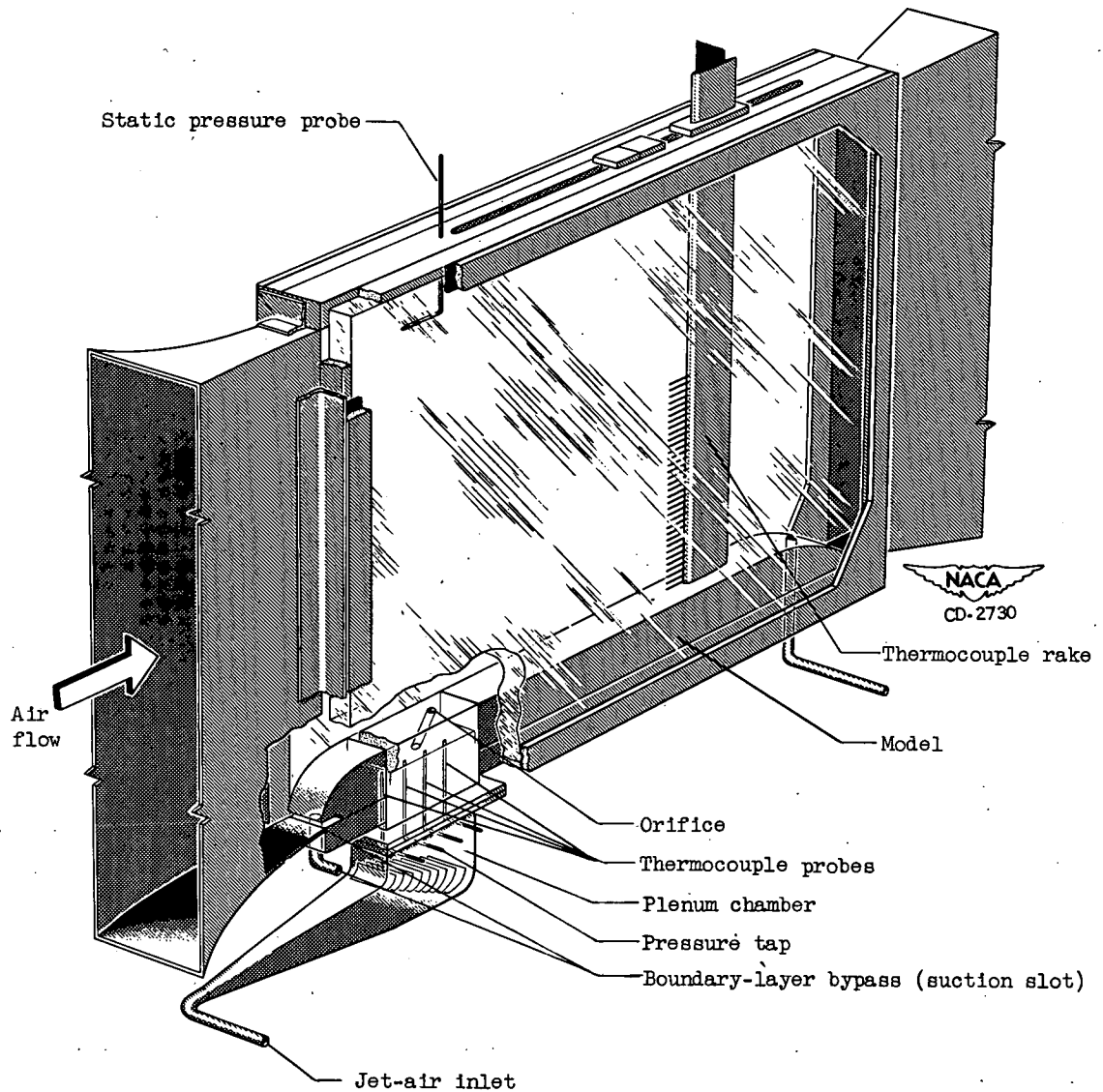
(a) Arrangement of orifice in plane parallel to air stream.

Figure 1. - Experimental arrangement used in investigation.
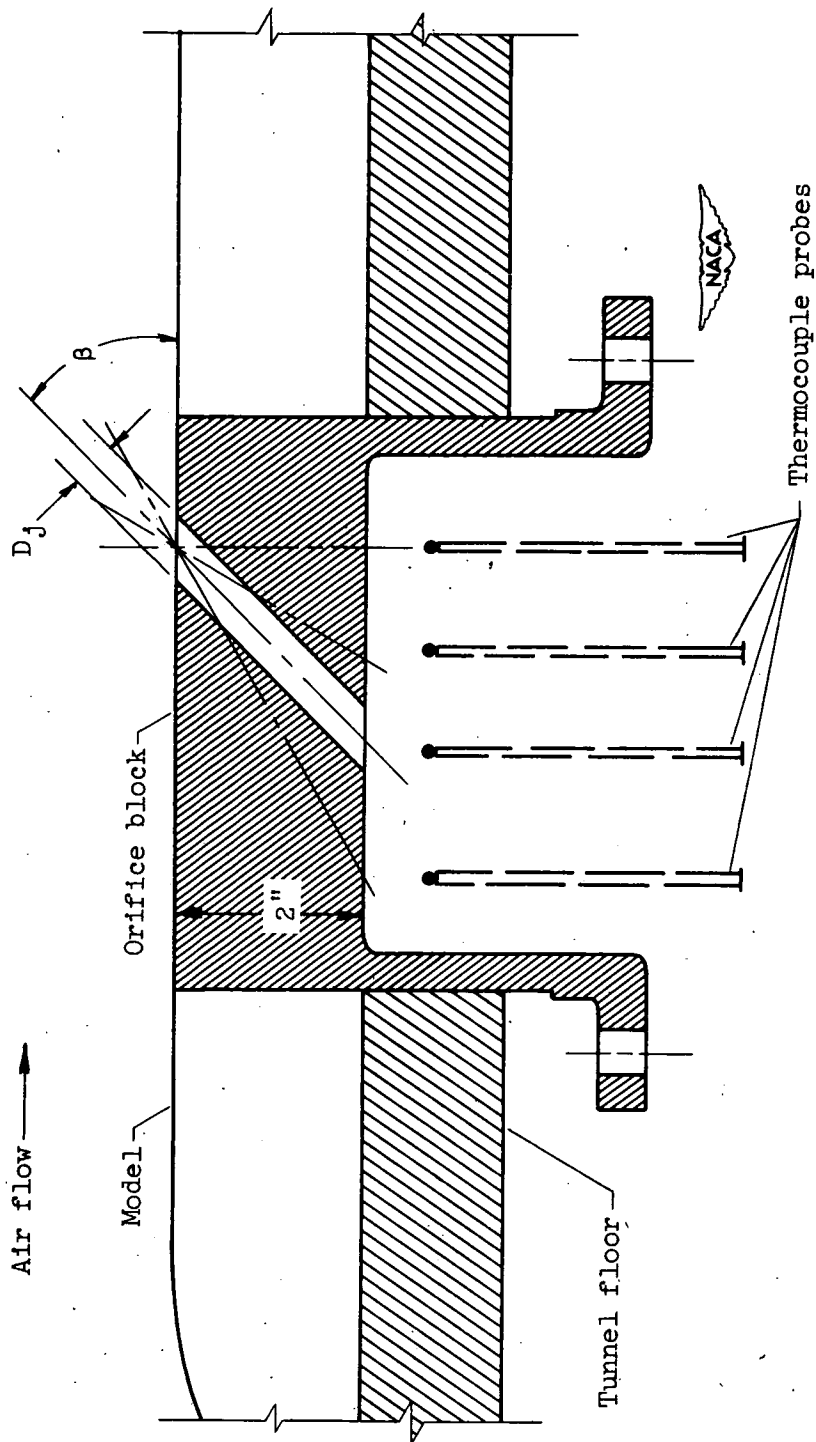
(b) Orifice mounted in plane parallel to air stream.

Figure 1. - Continued. Experimental arrangement used in investigation.
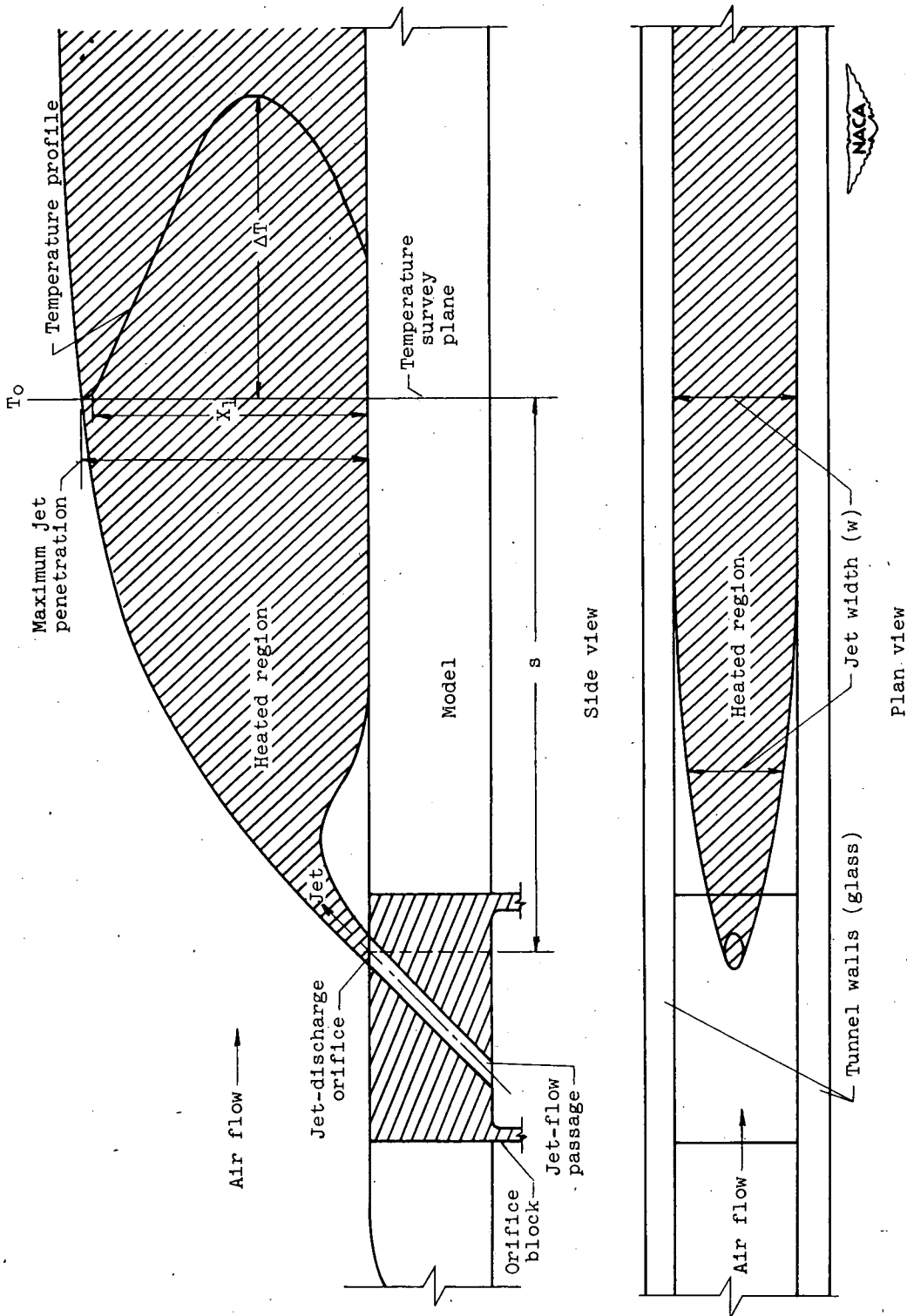
(c) Nomenclature and typical temperature profile produced by jet discharging at angle to air stream.

Figure 1. - Concluded. Experimental arrangement used in investigation.
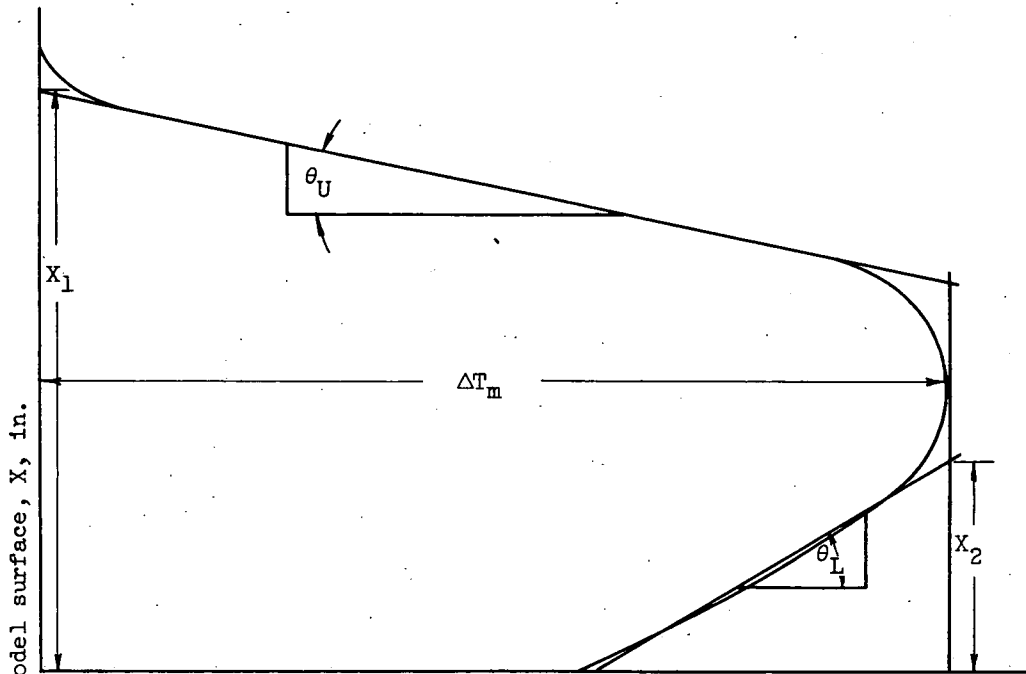
(a) Type I profile.
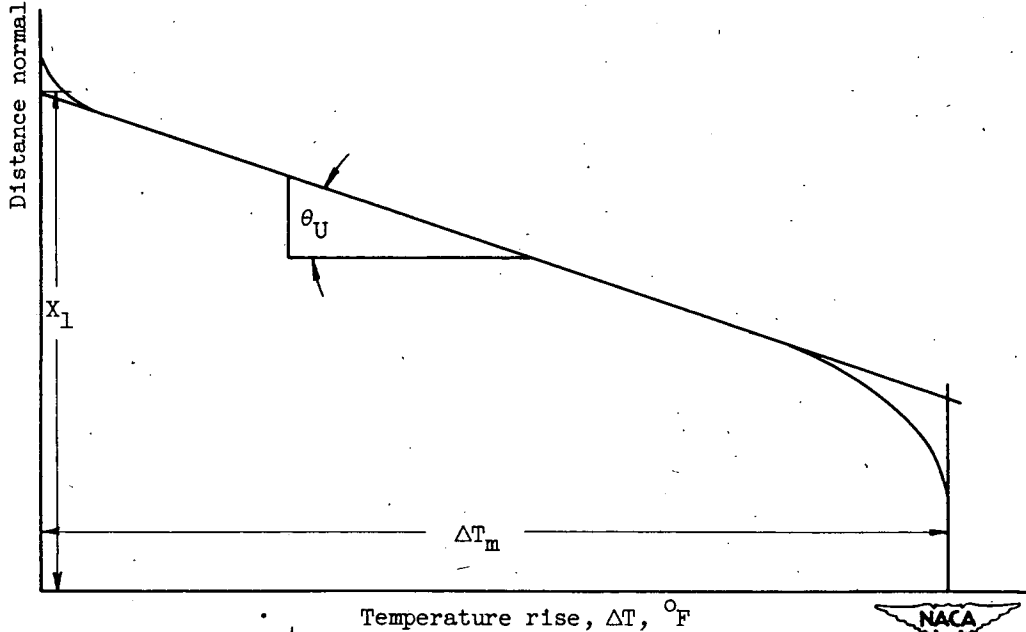
(b) Type II profile.

Figure 2. - Generalization of various types of temperature profile
showing penetrations X_1 and X_2, slopes $M_U = \tan \theta_U$ and
$M_L = \tan \theta_L$, maximum temperature rise ΔT_m, and temperature
rise ΔT_1.
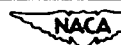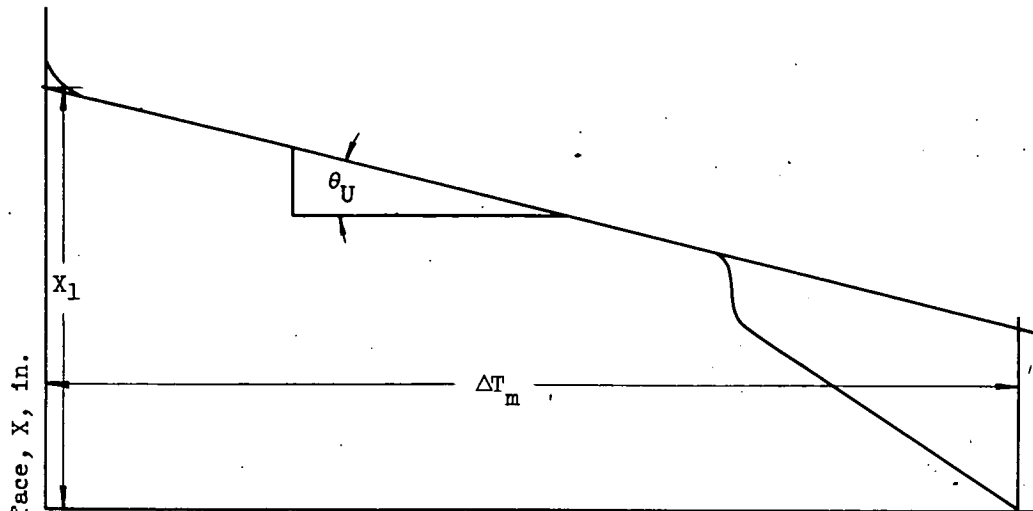
(c) Type III profile.
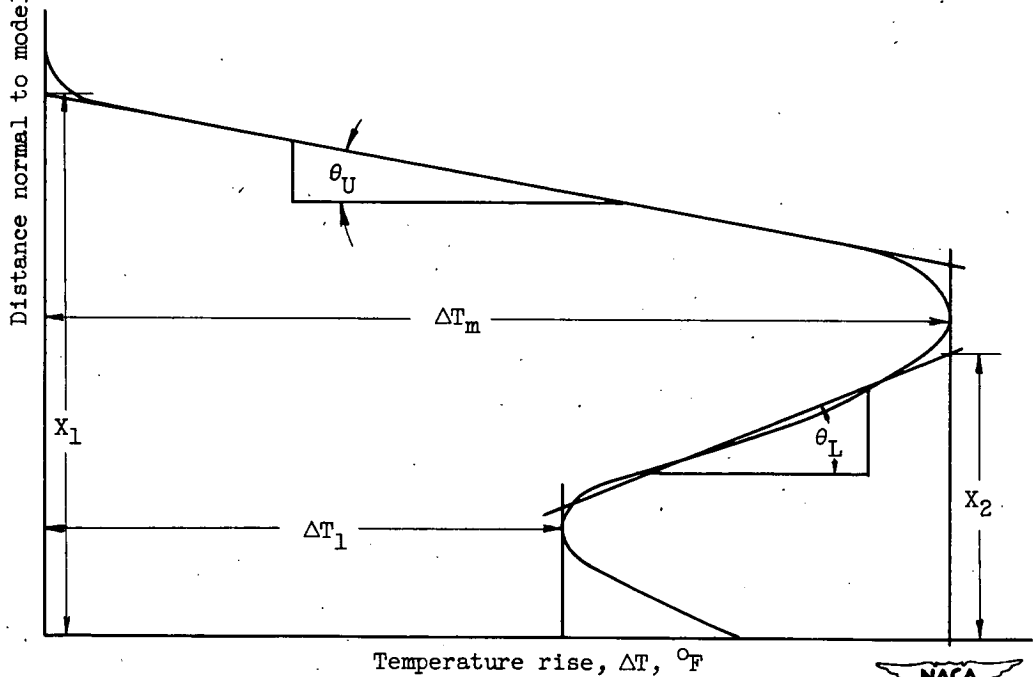
(d) Type IV profile.

Figure 2. - Concluded. Generalization of various types of temperature
profile showing penetrations X_1 and X_2, slopes $M_U = \tan \theta_U$ and
$M_L = \tan \theta_L$, maximum temperature rise ΔT_m, and temperature rise ΔT_1.
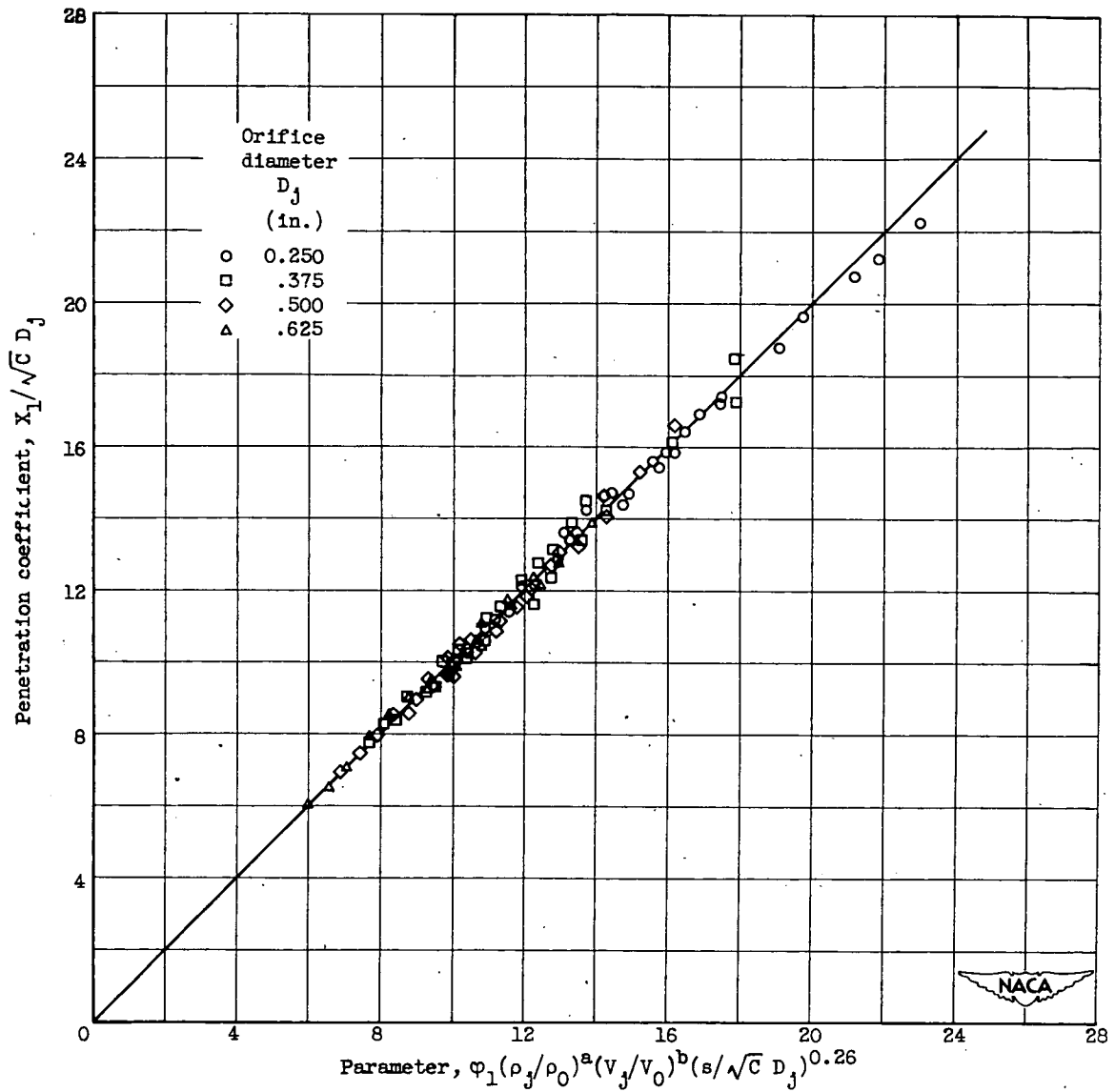
Figure 3. - Variation of penetration coefficient $X_1/\sqrt{C}\ D_j$ with parameter $\varphi_1(\rho_j/\rho_0)^a(V_j/V_0)^b(s/\sqrt{C}\ D_j)^{0.26}$. Jet angle, $90°$.
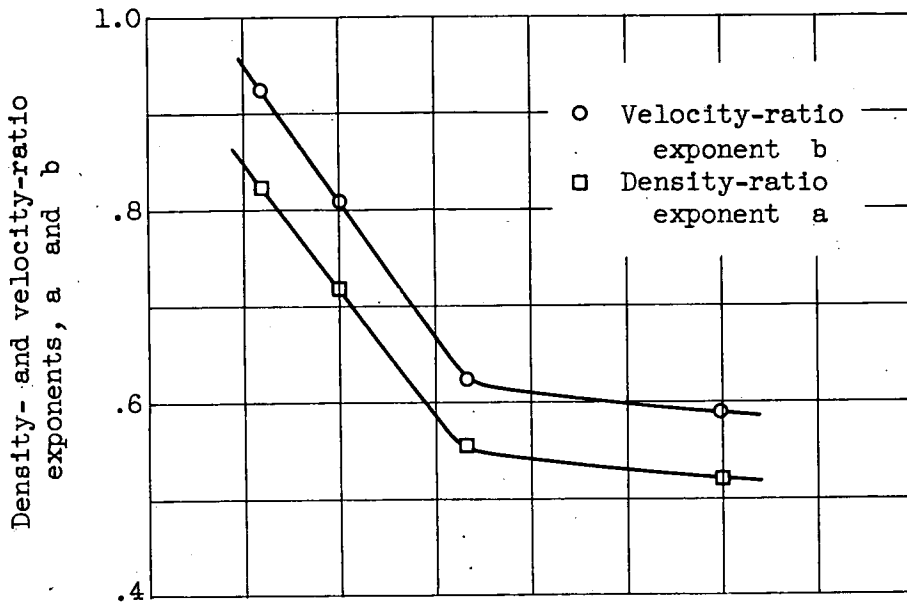
(a) Density- and velocity-ratio exponents.
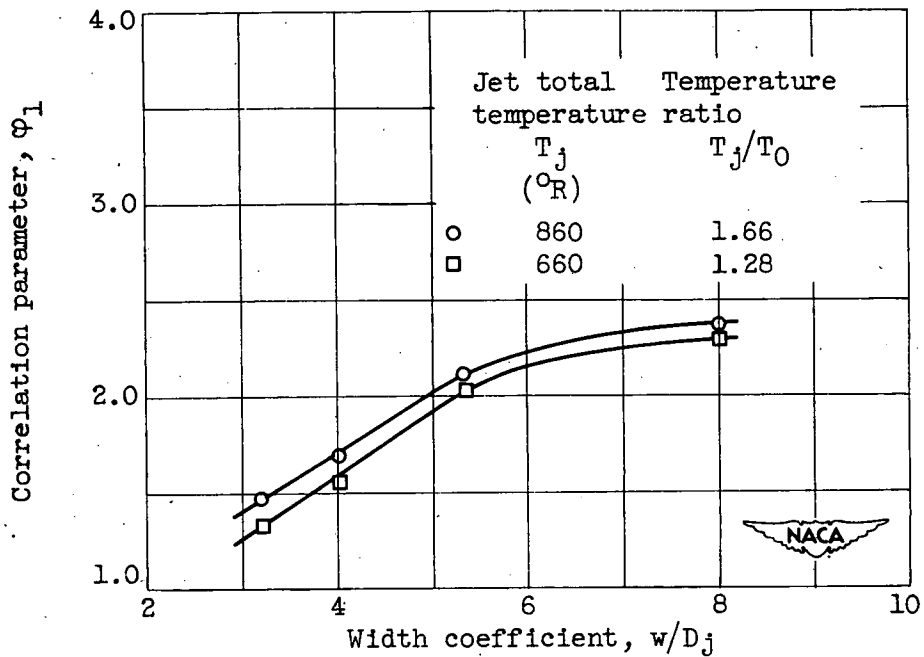
(b) Correlation parameter.

Figure 4. - Variation of density- and velocity-
ratio exponents a and b and correlation
parameter φ_1 with width coefficient. Jet
angle, $90°$.
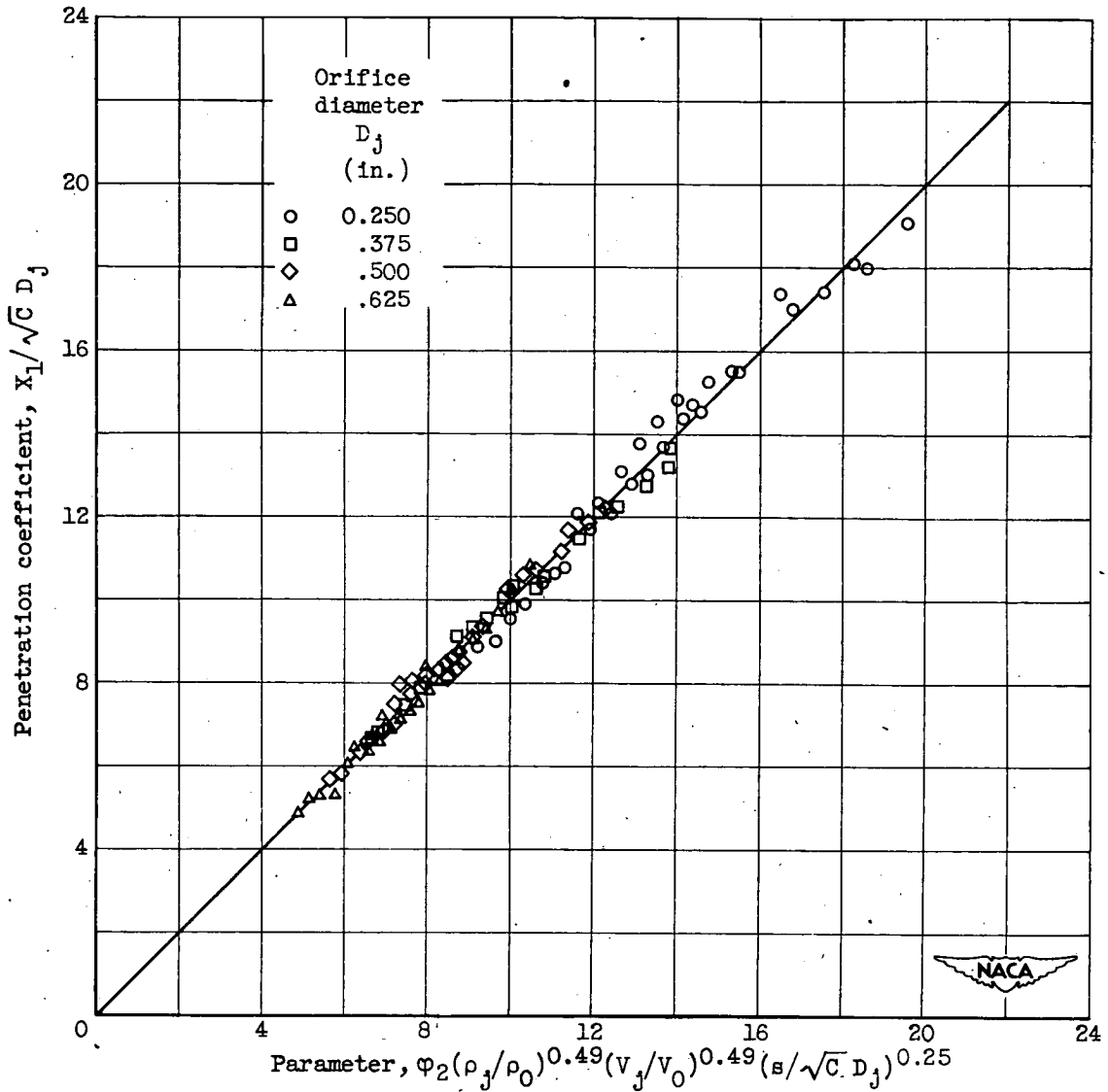
Figure 5. - Variation of penetration coefficient $X_1/\sqrt{C} \, D_j$ with parameter $\varphi_2(\rho_j/\rho_0)^{0.49}(V_j/V_0)^{0.49}(s/\sqrt{C} \, D_j)^{0.25}$. Jet angle, $60°$.
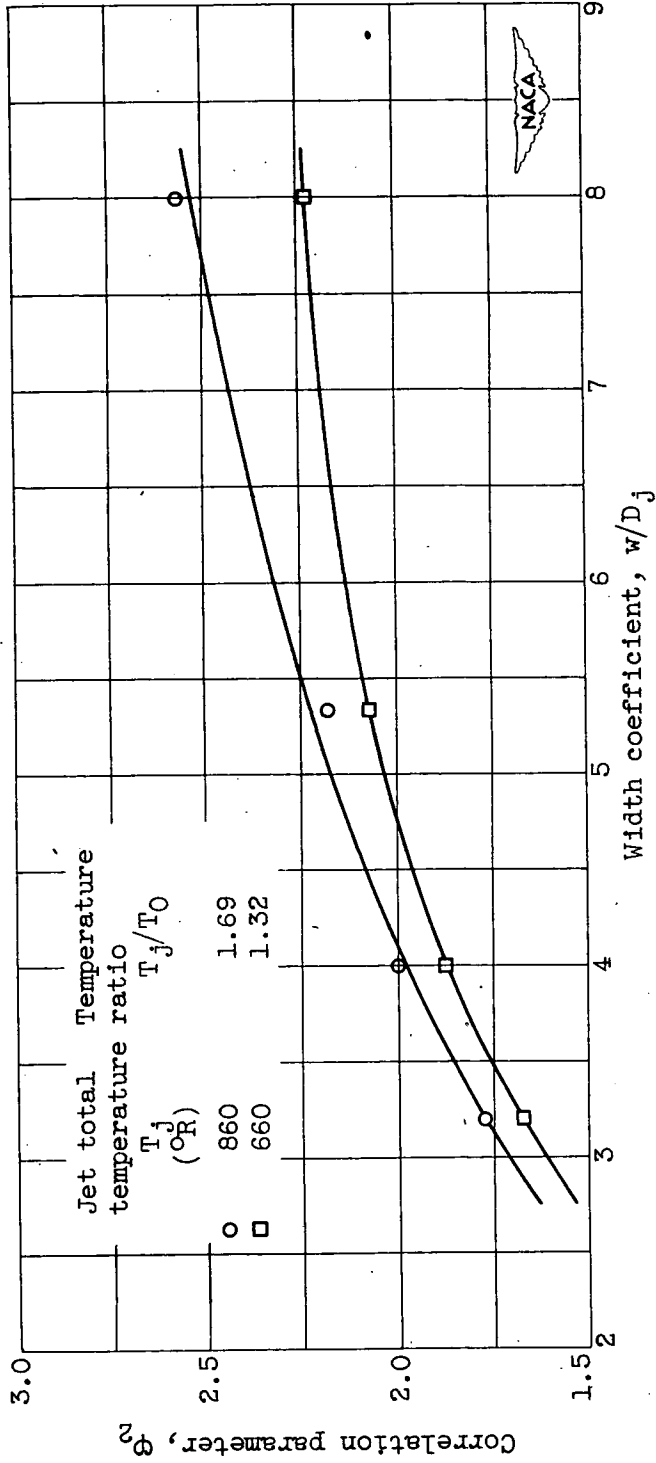
Figure 6. - Variation of correlation parameter φ_2 with width coefficient for constant values of temperature ratio. Jet angle, 60°.
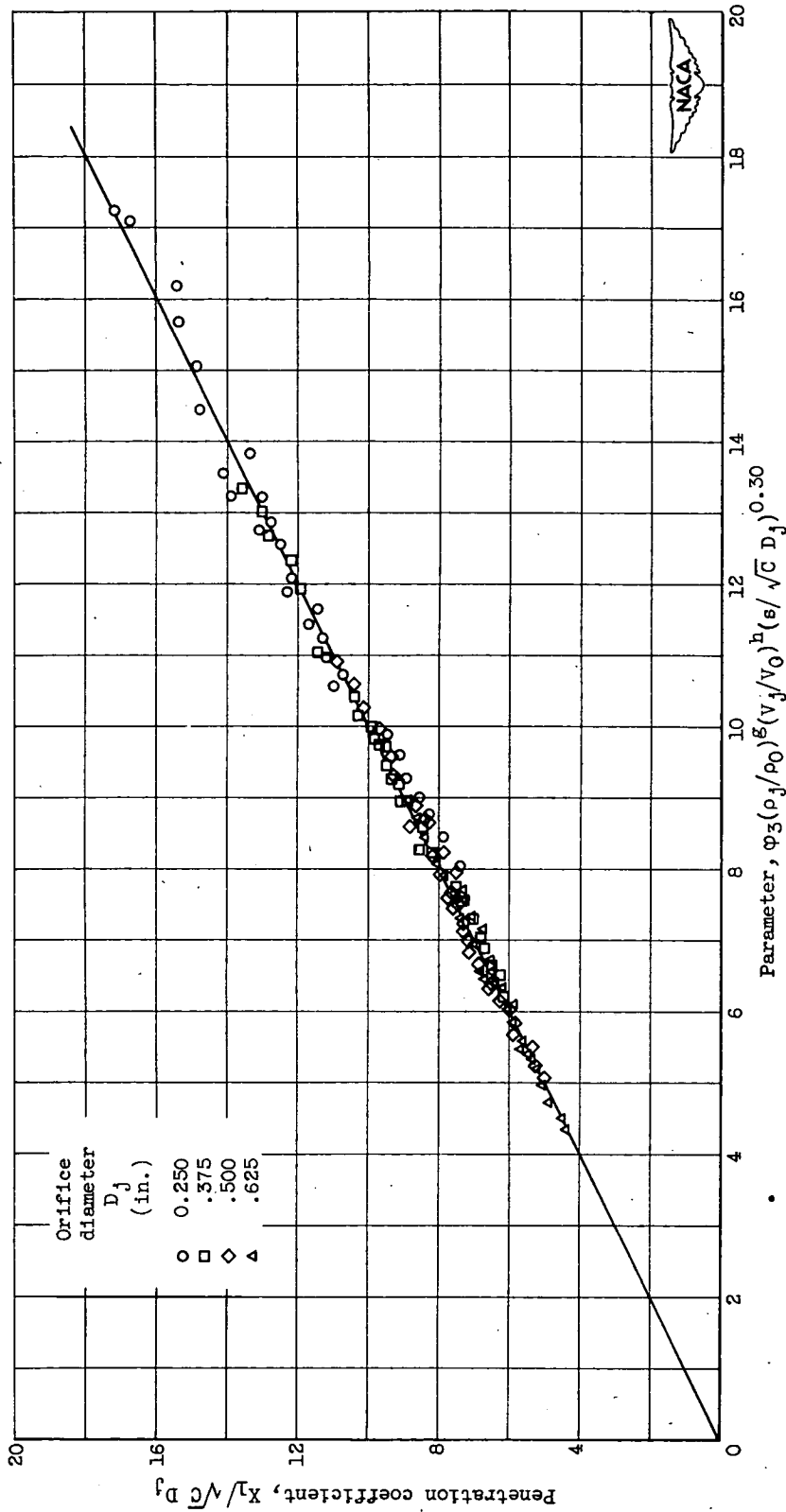
Figure 7. - Variation of penetration coefficient $x_l/\sqrt{C} D_j$ with parameter $\varphi_3(\rho_j/\rho_0)^g(v_j/v_0)^h(s/\sqrt{C} D_j)^{0.30}$. Jet angle, 45°.
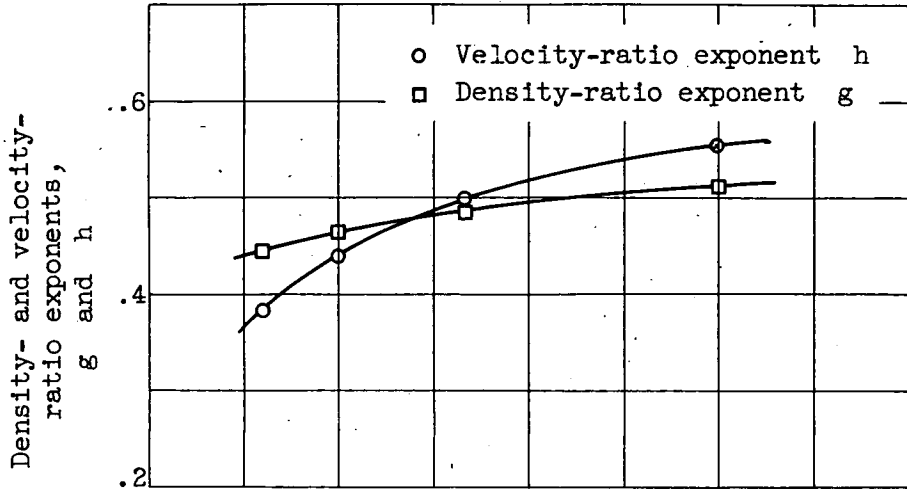
(a) Density- and velocity-ratio exponents.
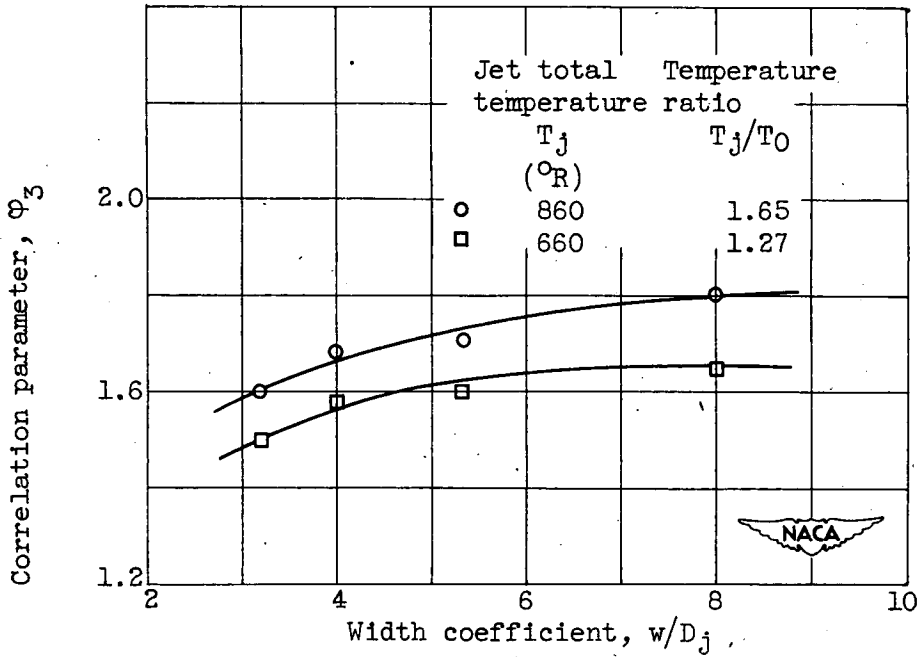
(b) Correlation parameter.

Figure 8. - Variation of density- and velocity-
ratio exponents g and h and correlation
parameter φ_3 with width coefficient. Jet
angle, 45°.
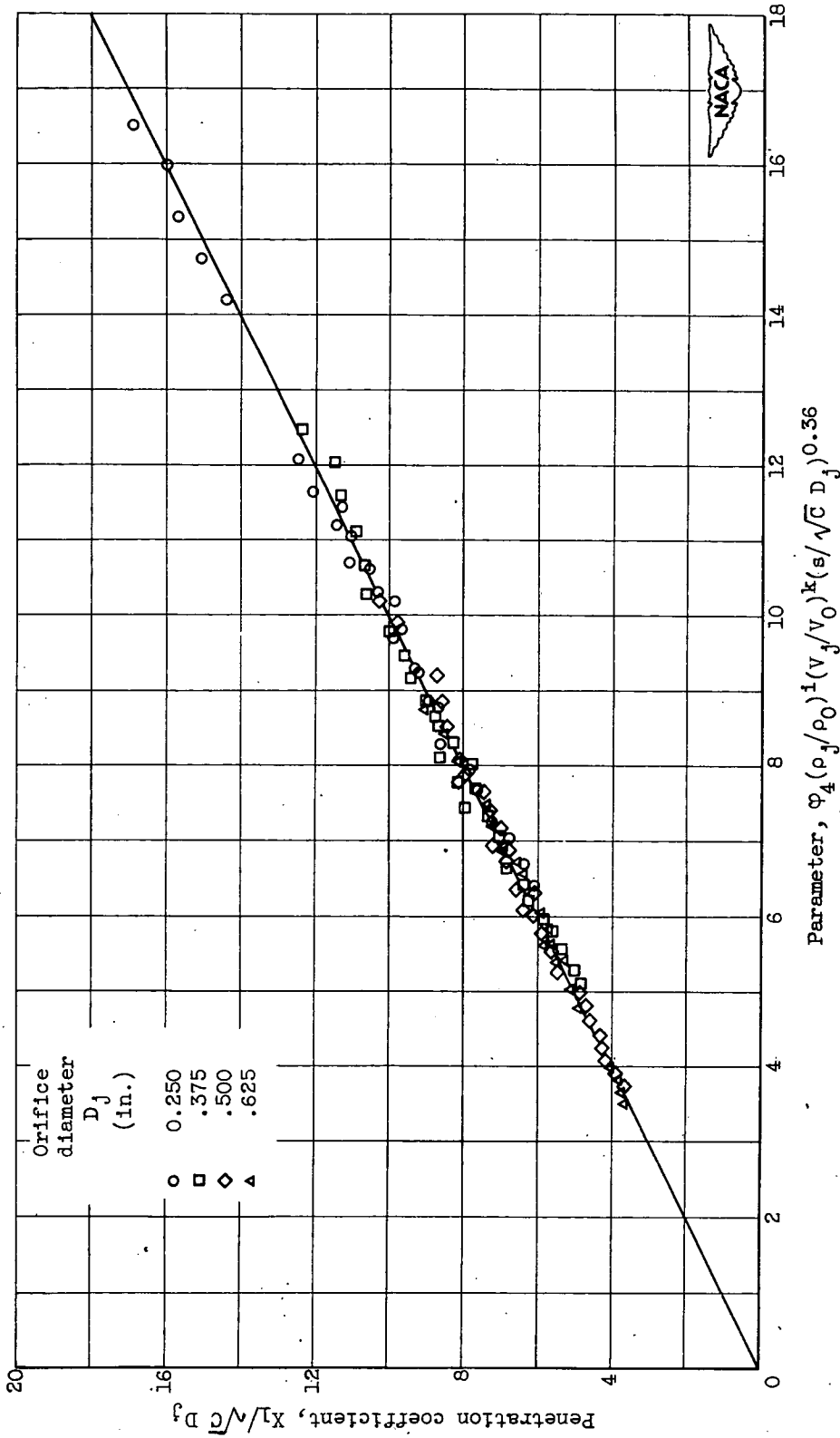
Figure 9. - Variation of penetration coefficient $X_1/\sqrt{C}\ D_j$, with parameter $\varphi_4(\rho_j/\rho_0)^i(v_j/v_0)^k(s/\sqrt{C}\ D_j)^{0.36}$. Jet angle, 30°.
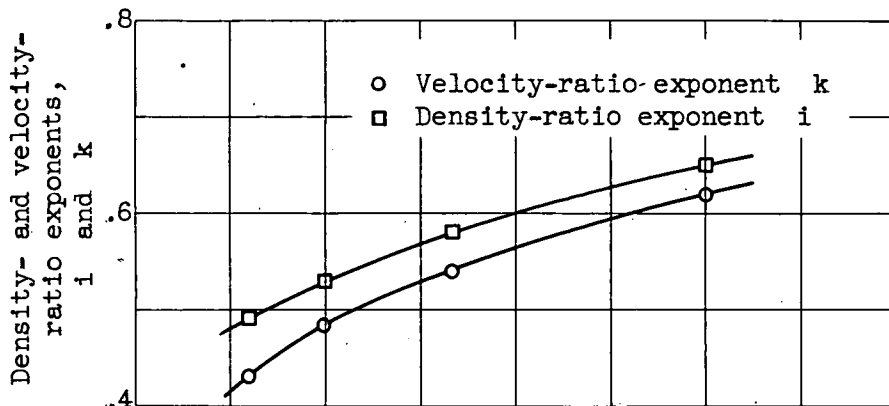
(a) Density- and velocity-ratio exponents.
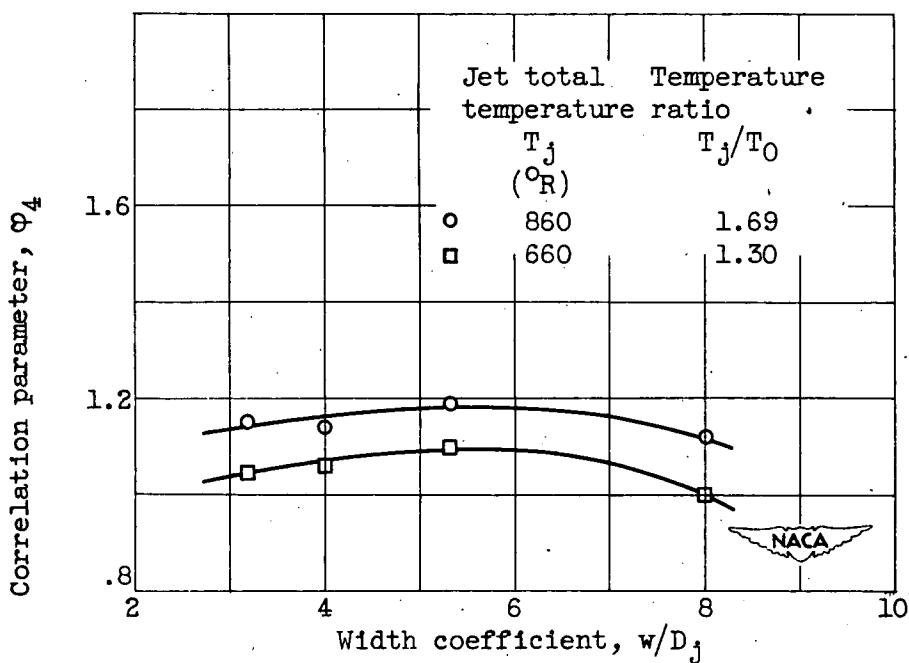
(b) Correlation parameter.

Figure 10. - Variation of density- and velocity-ratio exponents i and k and correlation parameter φ_4 with width coefficient. Jet angle, 30°.
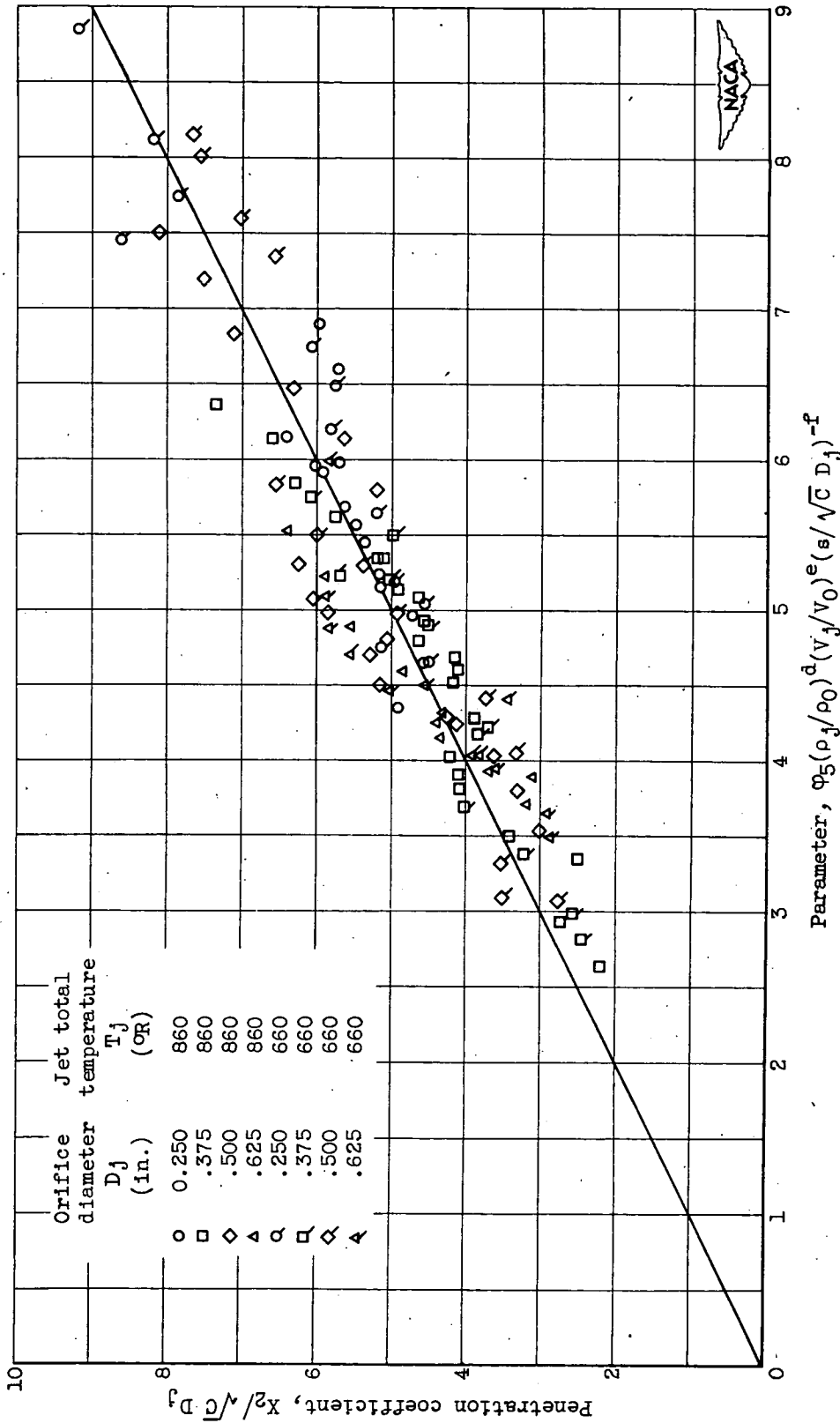
Figure 11. - Variation of penetration coefficient $x_2/\sqrt{C}\ D_j$ with parameter $\varphi_5(\rho_j/\rho_0)^d(V_j/V_0)^e(s/\sqrt{C}\ D_j)^{-f}$ for various jet total temperatures. Jet angle, 90°.
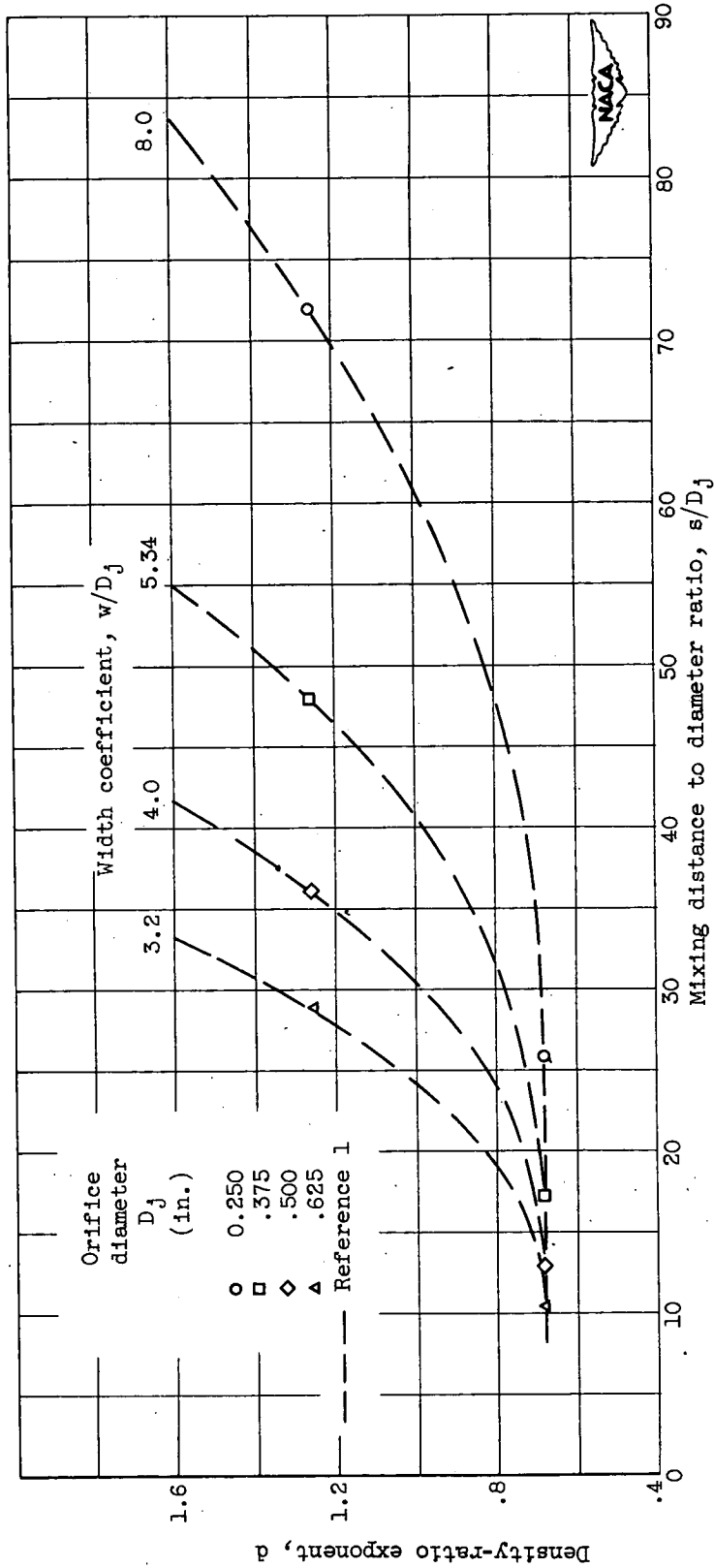
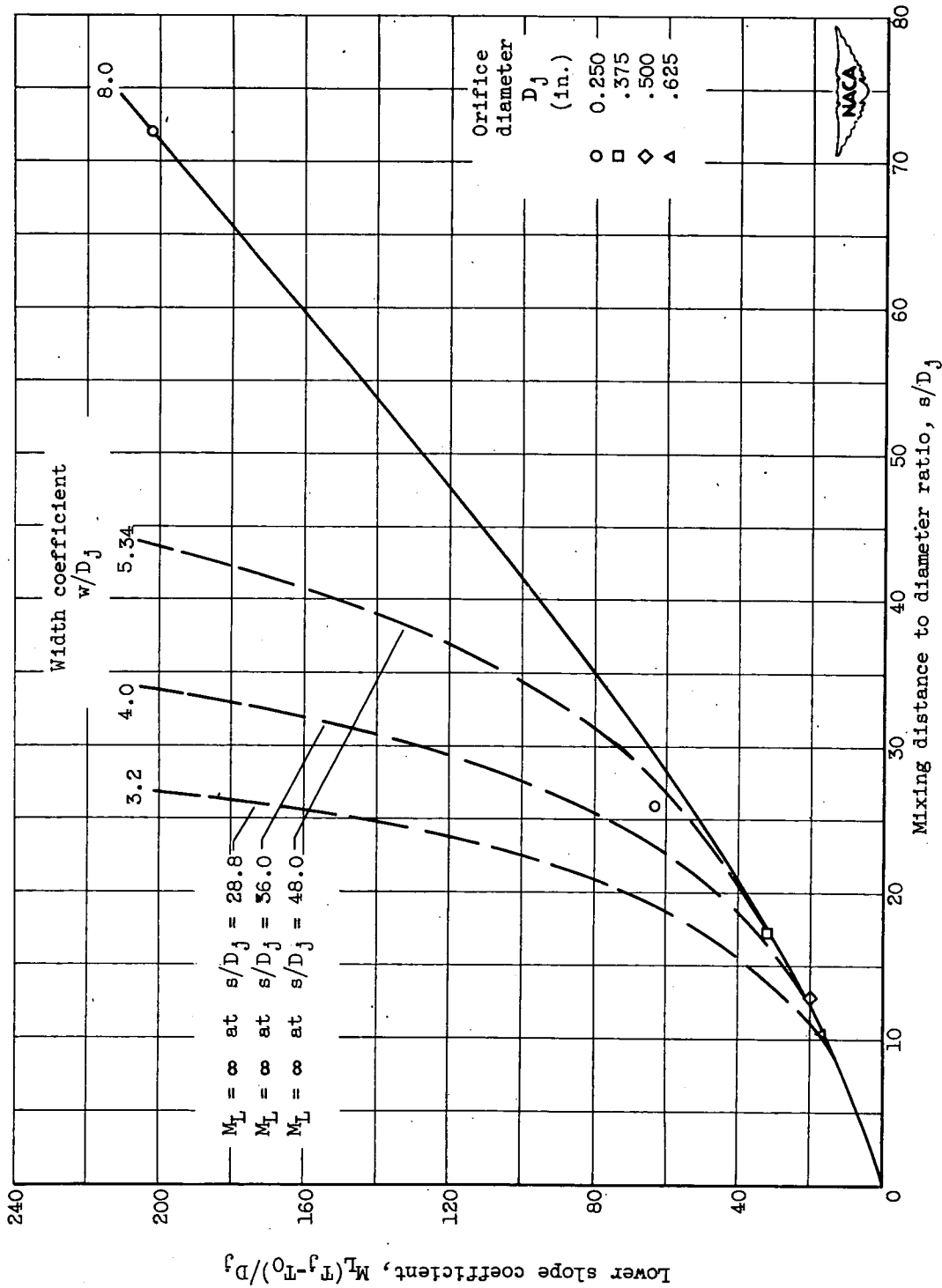Figure 12. – Variation of density-ratio exponent d with mixing distance to diameter ratio for constant values of width coefficient. Jet angle, 60°.
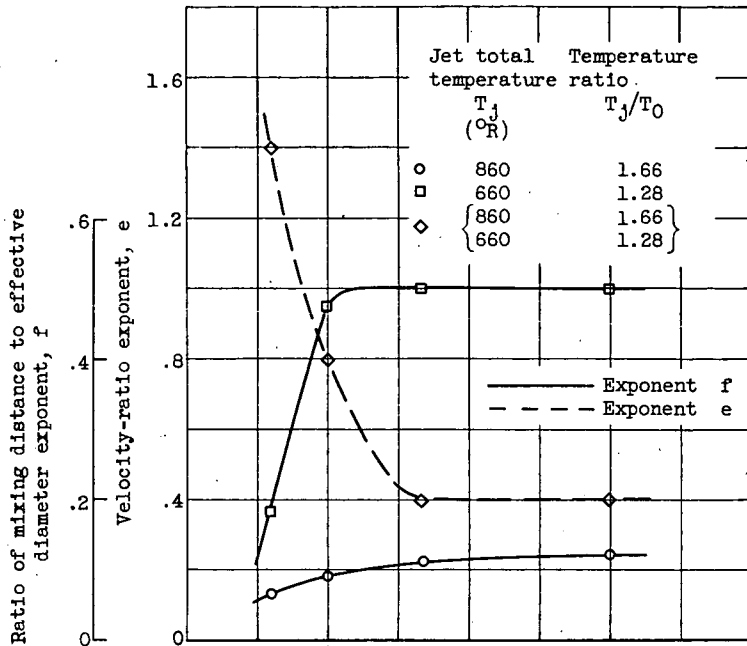
(a) Velocity-ratio and ratio of mixing distance
to effective diameter exponents.
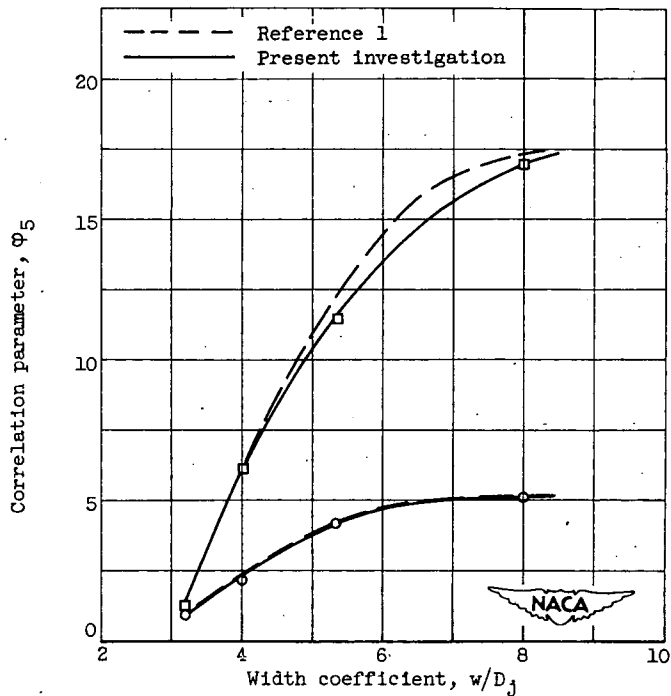
(b) Correlation parameter.

Figure 13. - Variation of velocity-ratio expo-
nent e, ratio of mixing distance to effective
diameter exponent f, and correlation param-
eter φ_5 with width coefficient. Jet angle,
90°.
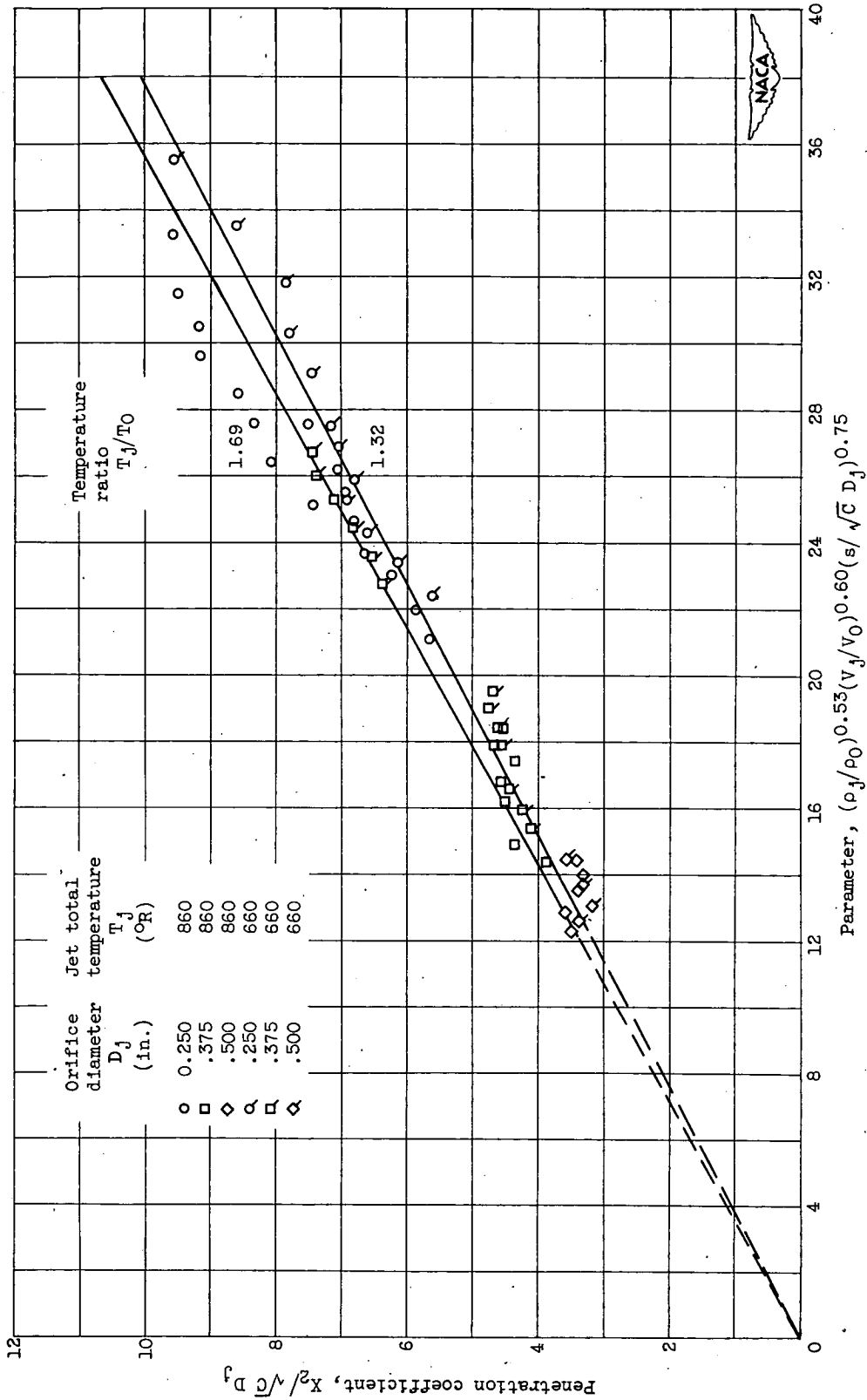
Figure 14. - Variation of penetration coefficient $X_2/\sqrt{C}\ D_j$ with parameter $(\rho_j/\rho_0)^{0.53}(v_j/v_0)^{0.60}(s/\sqrt{C}\ D_j)^{0.75}$ for constant values of temperature ratio. Jet angle, 60°.
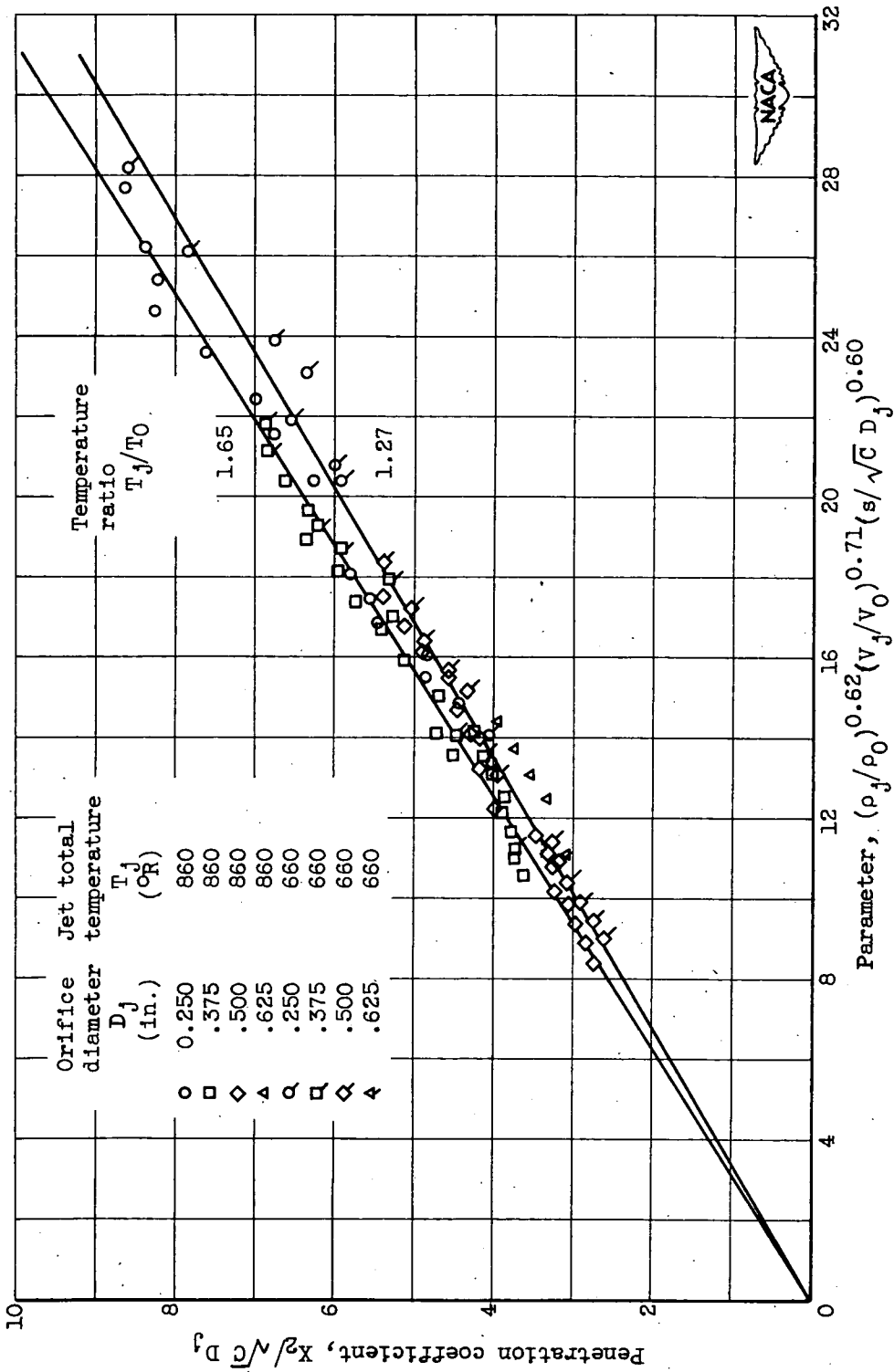
Figure 15. - Variation of penetration coefficient $X_2/\sqrt{C} \, D_j$ with parameter $(\rho_j/\rho_0)^{0.62}(V_j/V_0)^{0.71}(s/\sqrt{C} \, D_j)^{0.60}$ for constant values of temperature ratio. Jet angle, 45°.
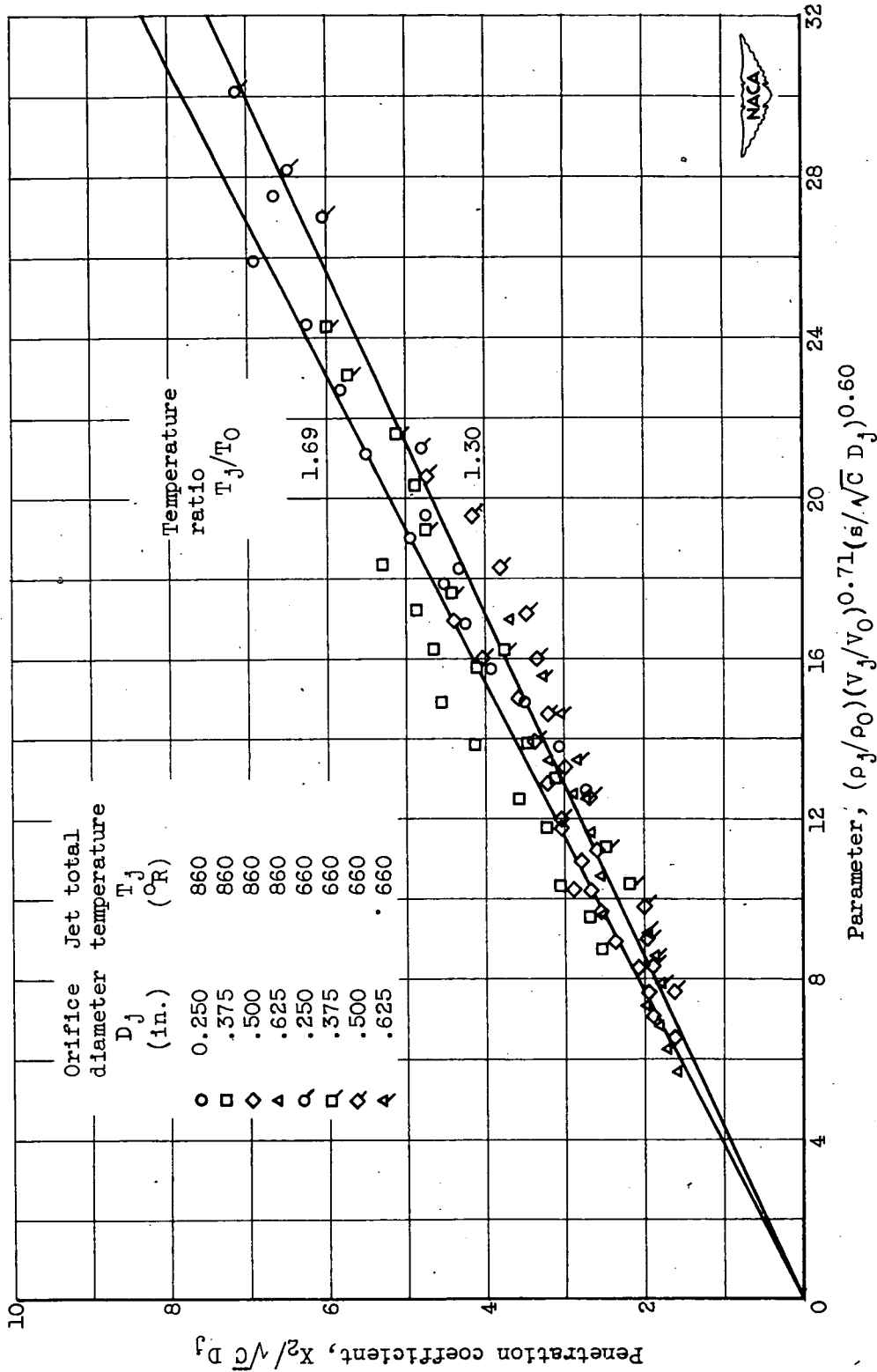
Figure 16. - Variation of penetration coefficient $X_2/\sqrt{C} \, D_j$ with parameter $(\rho_j/\rho_0)(V_j/V_0)^{0.71}(s/\sqrt{C} \, D_j)^{0.60}$ for constant values of temperature ratio. Jet angle, 30°.
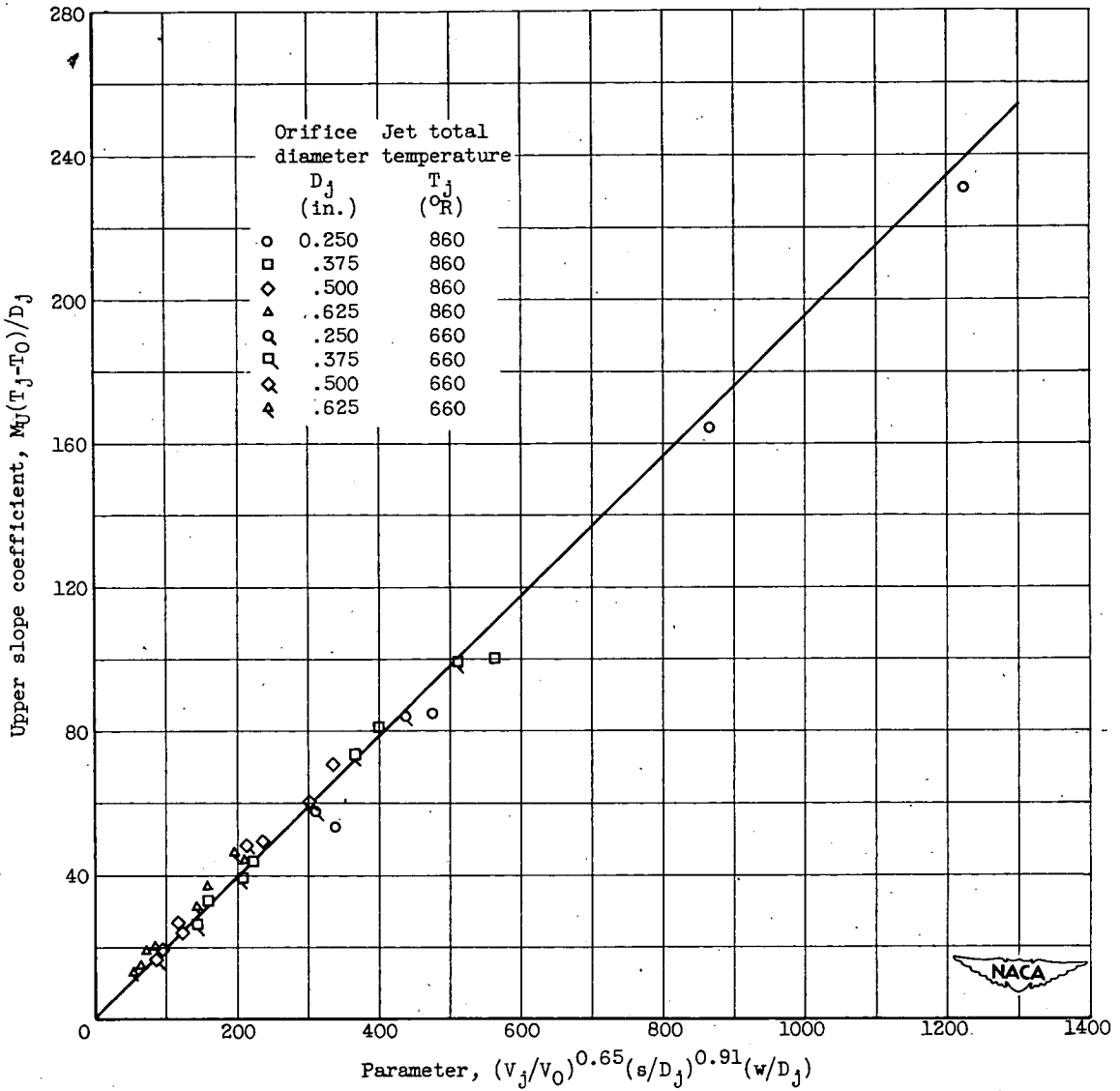
Figure 17. - Variation of upper slope coefficient with parameter
$(V_j/V_0)^{0.65}(s/D_j)^{0.91}(w/D_j)$. Jet angle, 90°.
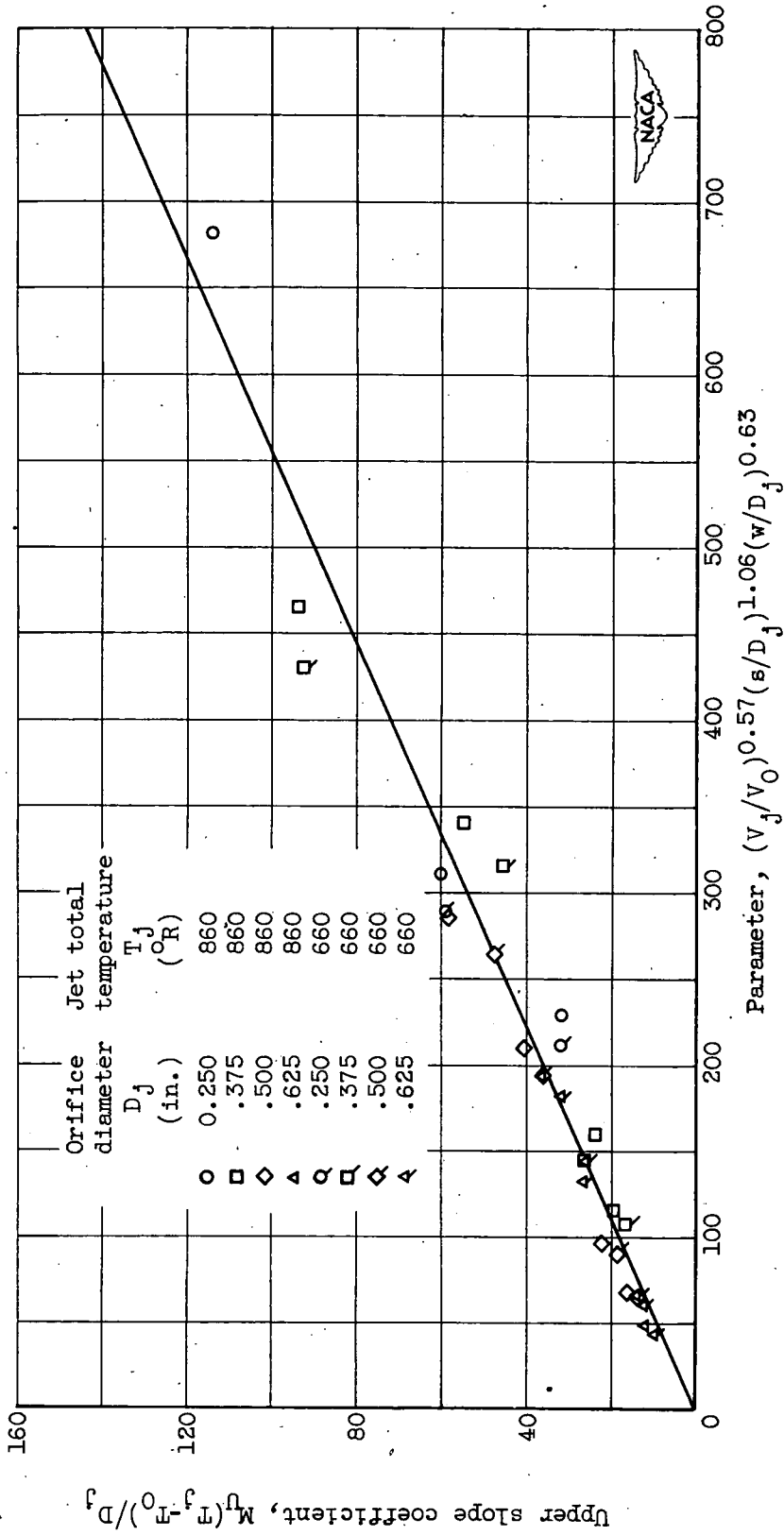
Figure 18. - Variation of upper slope coefficient with parameter $(V_j/V_0)^{0.57}(s/D_j)^{1.06}(w/D_j)^{0.63}$. Jet angle, 60°.
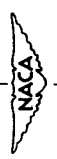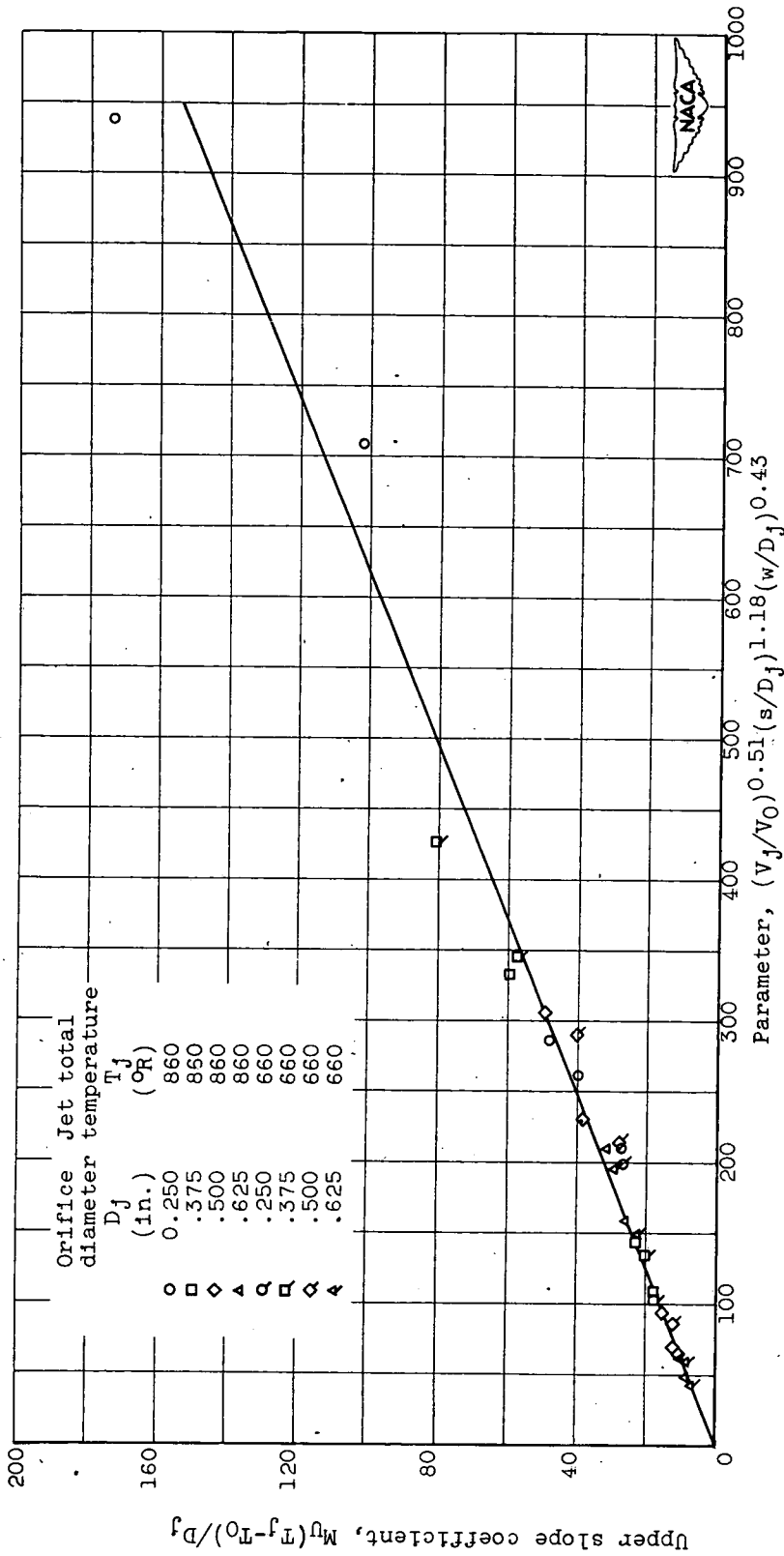
Figure 19. - Variation of upper slope coefficient with parameter $(V_j/V_0)^{0.51}(s/D_j)^{1.18}(w/D_j)^{0.43}$. Jet angle, 45°.
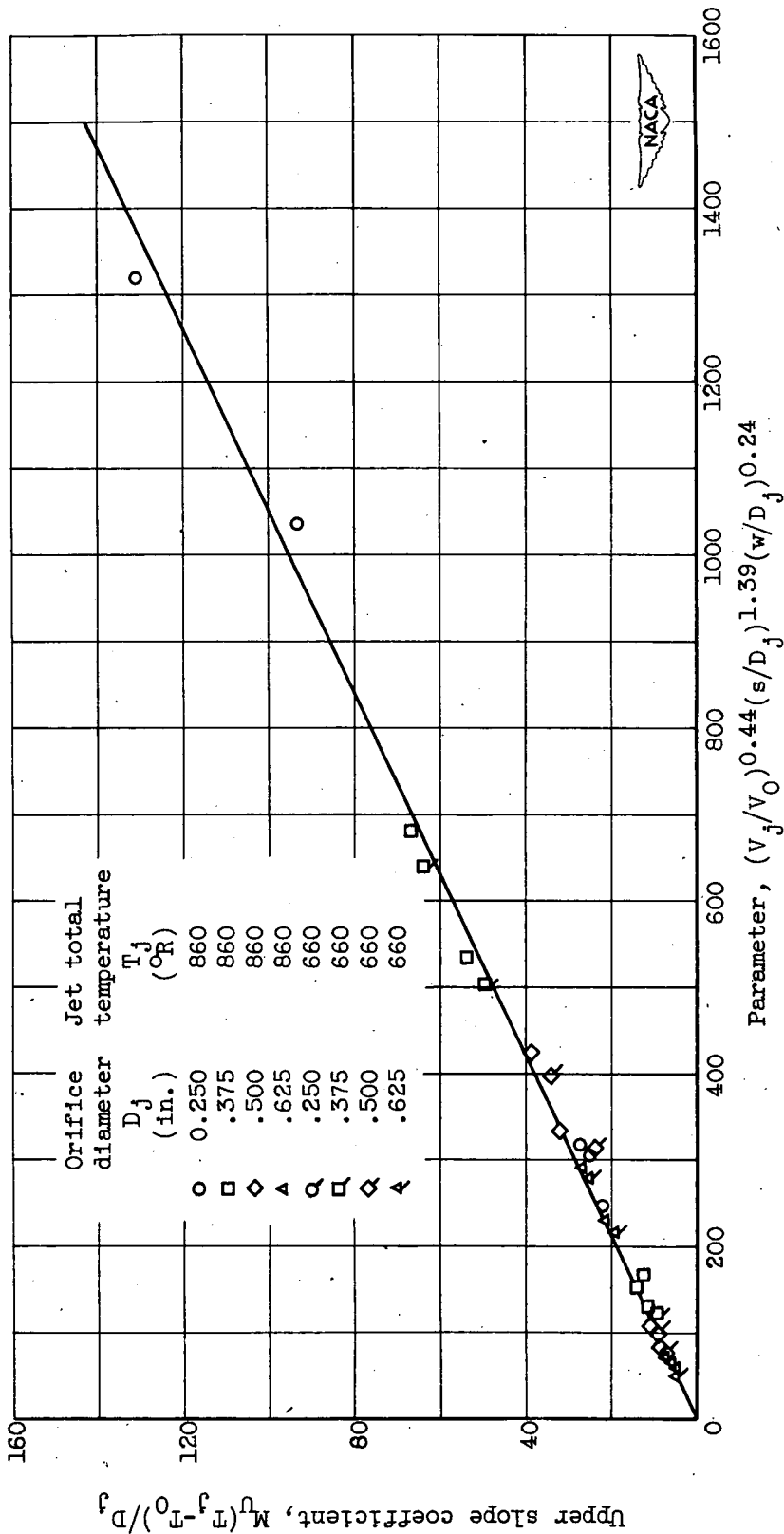
Figure 20. - Variation of upper slope coefficient with parameter $(V_j/V_0)^{0.44}(s/D_j)^{1.39}(w/D_j)^{0.24}$. Jet angle, 30°.
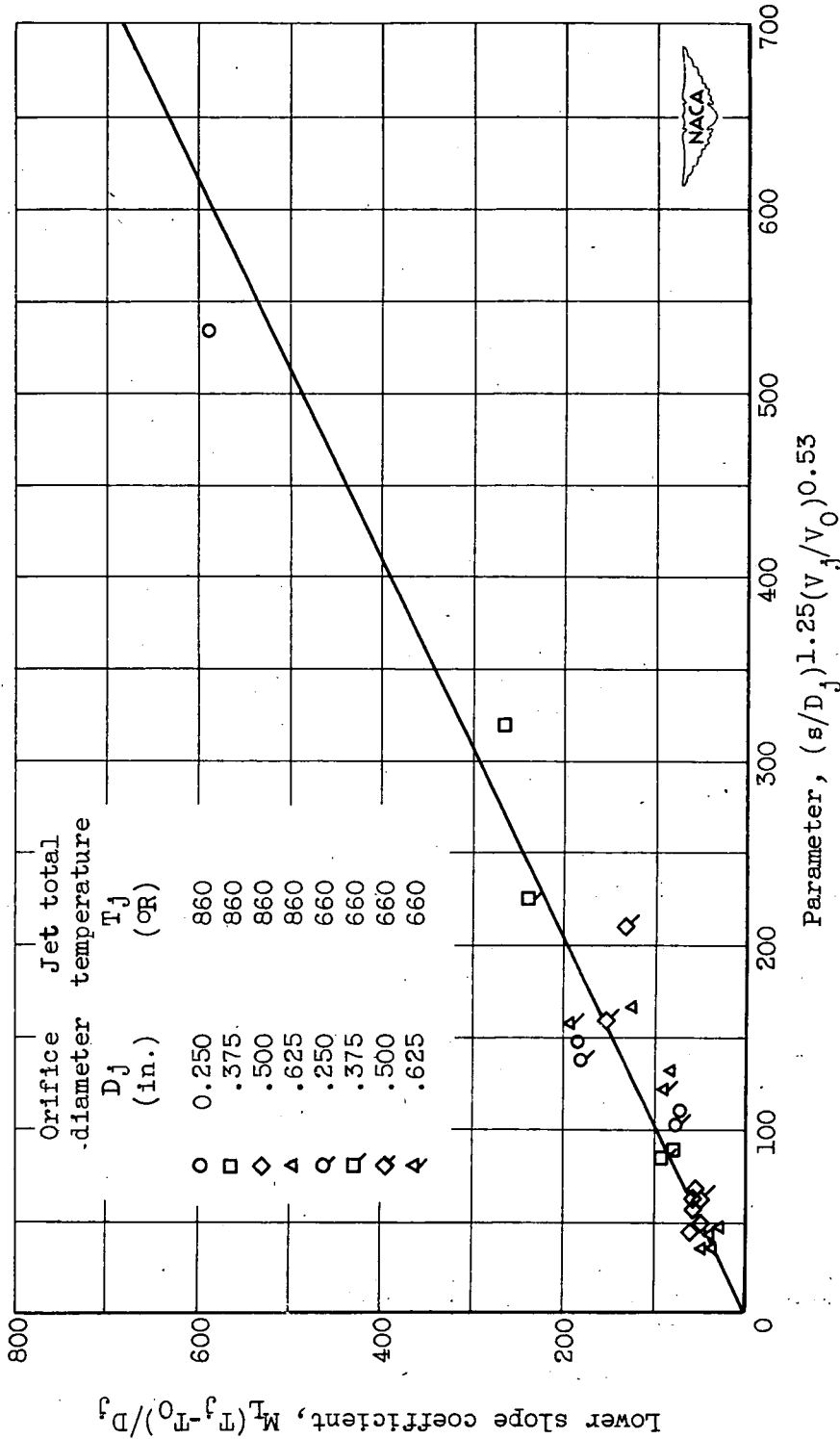
Figure 21. - Variation of lower slope coefficient with parameter $(s/D_j)^{1.25}(V_j/V_O)^{0.53}$ for various jet total temperatures. Jet angle, 90°.
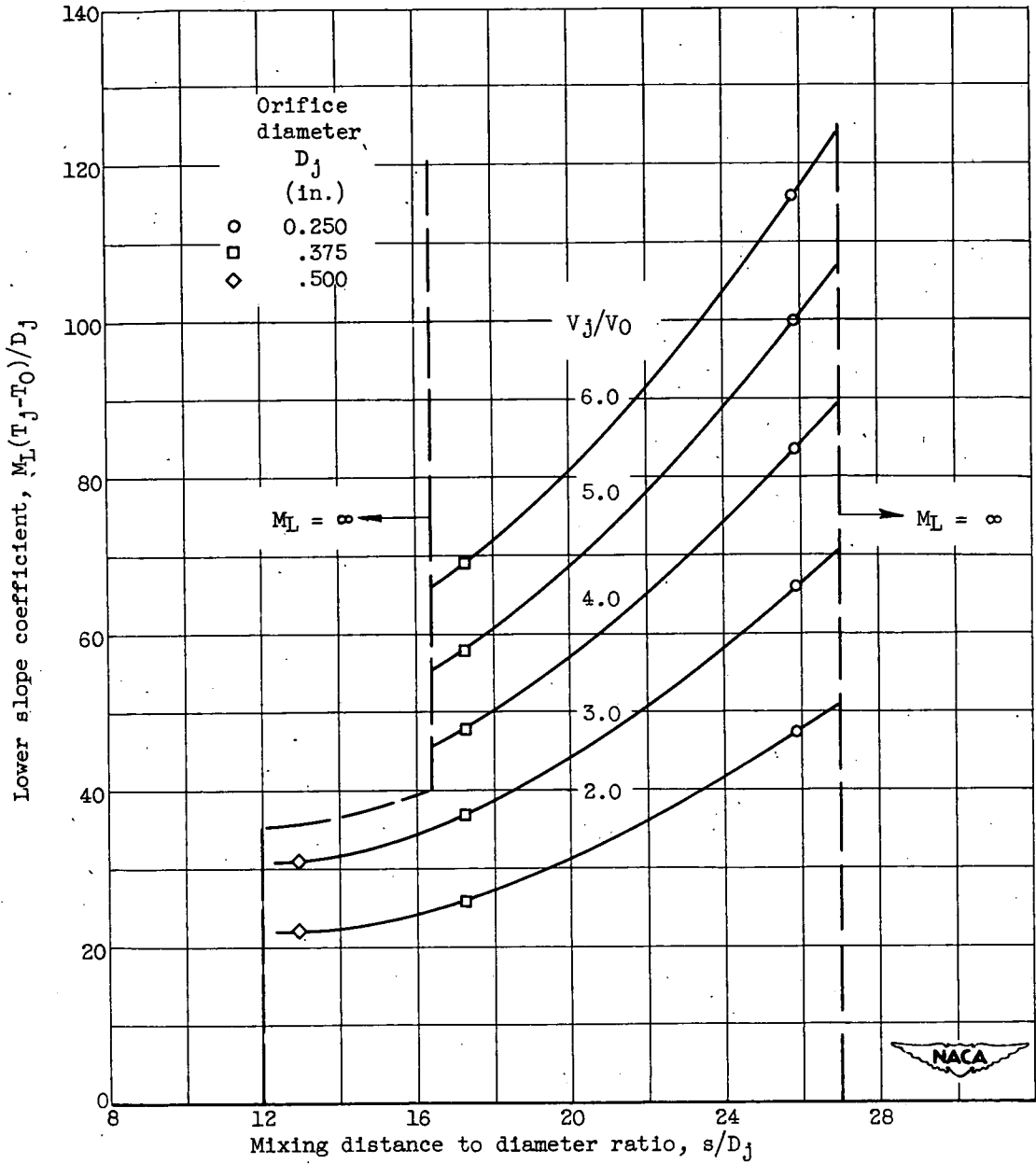
Figure 22. - Variation of lower slope coefficient with mixing distance to diameter ratio for constant values of velocity ratio. Jet angle, 60°.

Figure 23. - Variation of lower slope coefficient with mixing distance to diameter ratio for constant values of width coefficient. Jet angle, 45°.
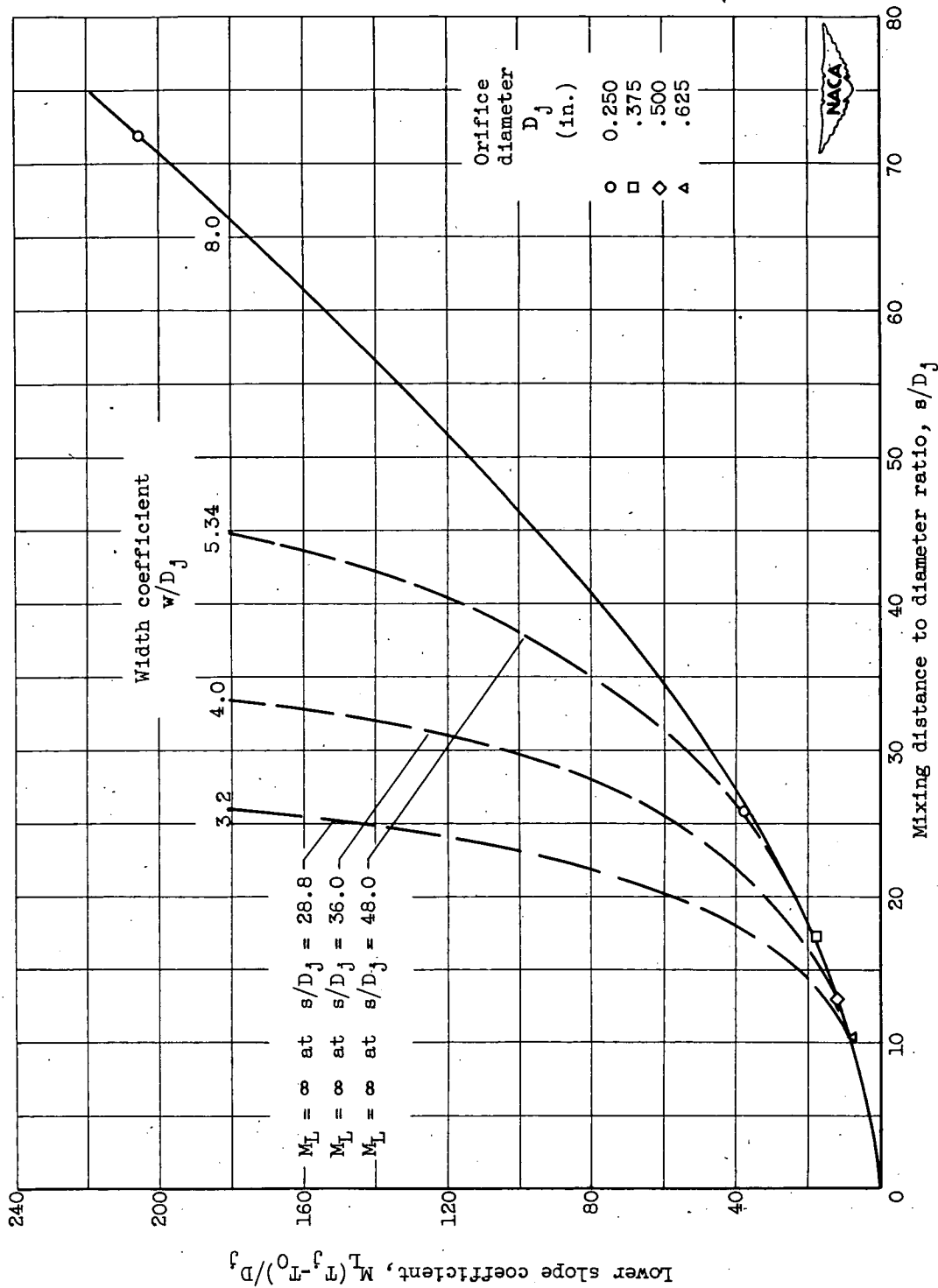
Figure 24. - Variation of lower slope coefficient with mixing distance to diameter ratio for constant values of width coefficient. Jet angle, 30°.
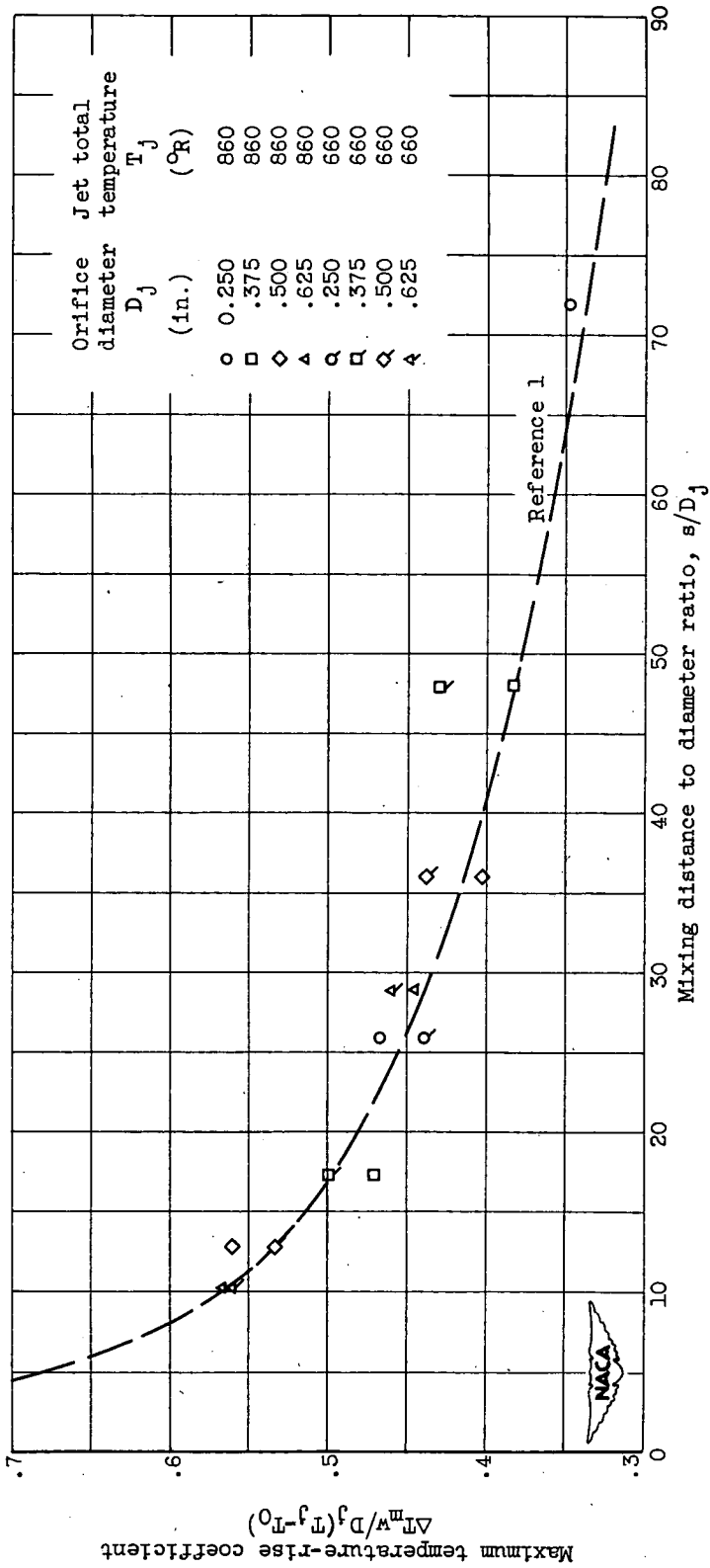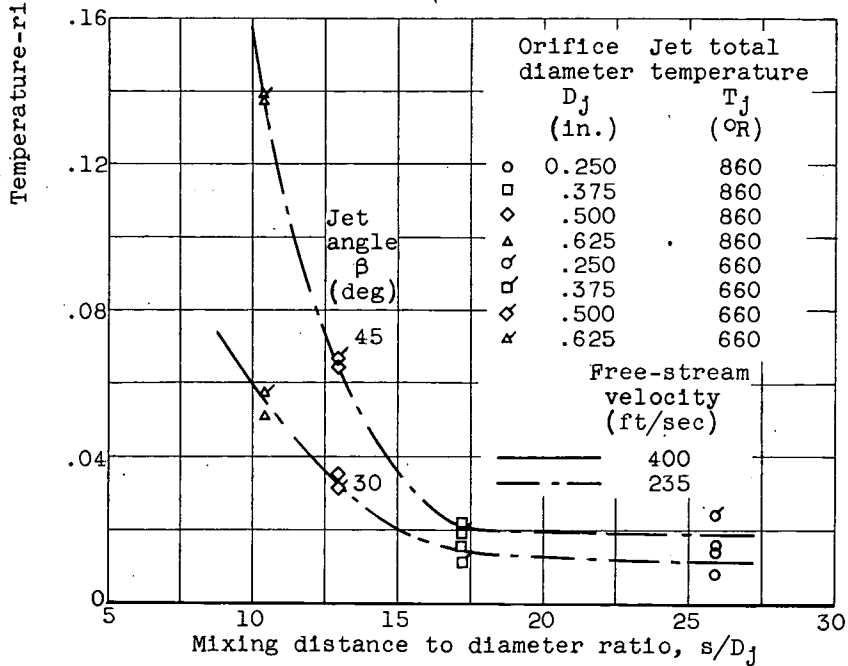
Figure 25. - Variation of maximum temperature-rise coefficient $\Delta T_m w / D_j (T_j - T_0)$ with mixing distance to diameter ratio. Jet angle, $90°$.
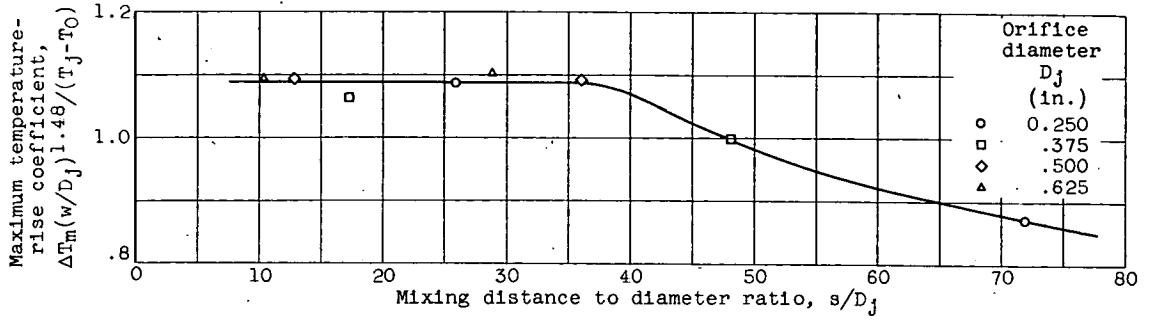
Figure 26. - Variation of maximum temperature-rise coefficient $\Delta T_m(w/D_j)^{1.48}/(T_j-T_0)$ with mixing distance to diameter ratio. Jet angle, 60°.
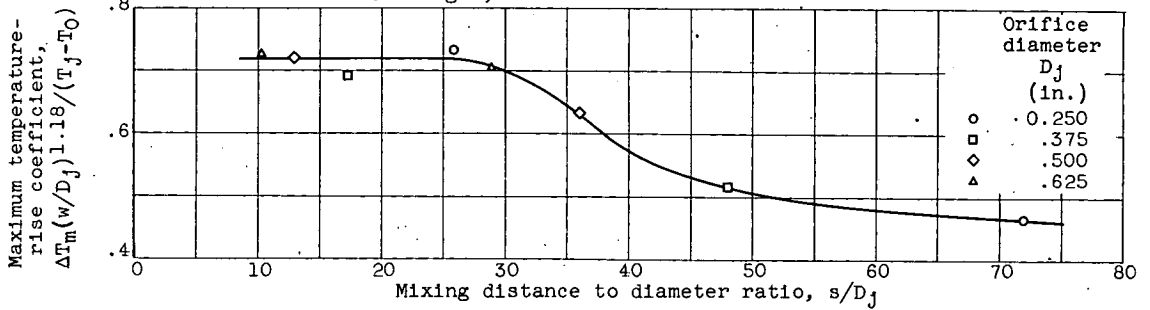

Figure 27. - Variation of maximum temperature-rise coefficient $\Delta T_m(w/D_j)^{1.18}/(T_j-T_0)$ with mixing distance to diameter ratio. Jet angle, 45°.
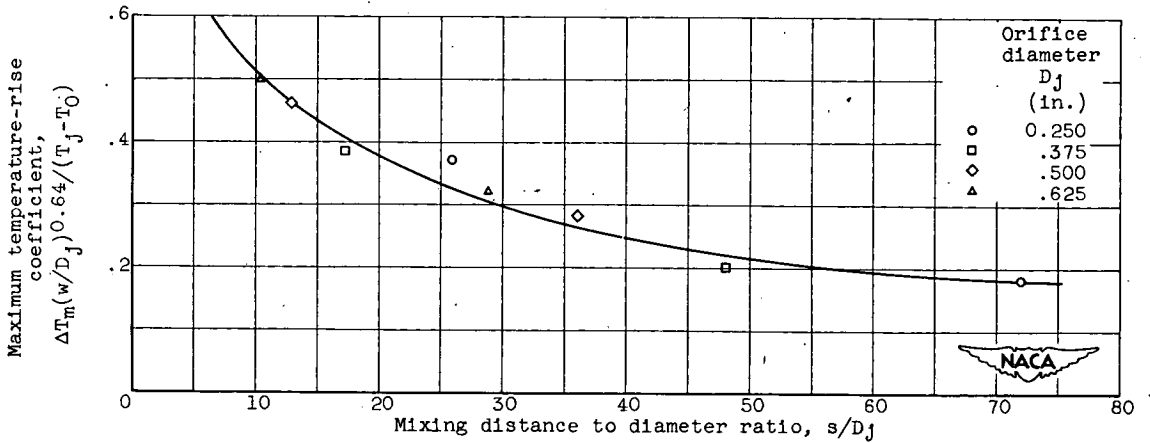
Figure 28. - Variation of maximum temperature-rise coefficient $\Delta T_m(w/D_j)^{0.64}/(T_j-T_0)$ with mixing distance to diameter ratio. Jet angle, 30°.

(a) Jet angle, 60°.

Orifice diameter D_j (in.)	Jet total temperature T_j (°R)
o 0.250	860
□ .375	860
◇ .500	860
△ .625	860
o' .250	660
□' .375	660
◇' .500	660
△' .625	660

Free-stream velocity (ft/sec)	
——————	400
—·—·—·—	235

Jet angle β (deg)
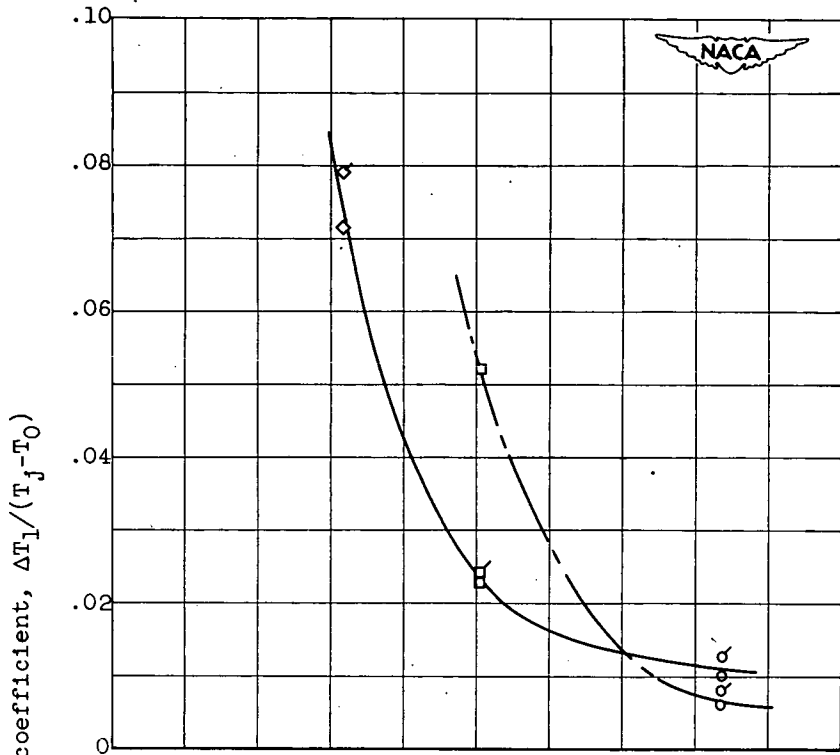
(b) Jet angles, 45° and 30°.

Figure 29. - Variation of temperature-rise coefficient with mixing distance to diameter ratio for jet angles of 60°, 45°, and 30°.

50

NACA TN 2855
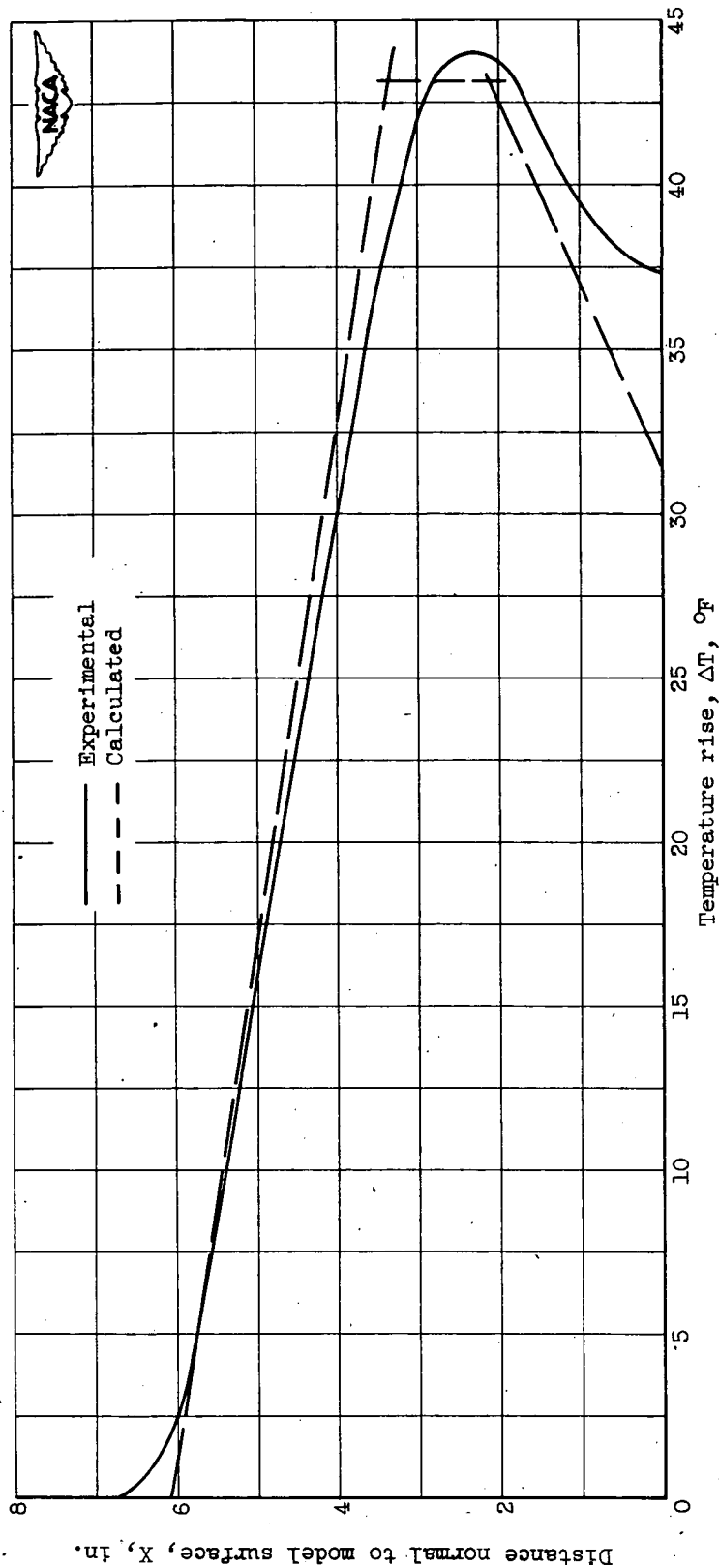
(a) Orifice diameter, 0.625 inch; jet total temperature, 860° R; jet pressure ratio, 2.38; free-stream velocity, 380 feet per second; rake position, 18.0 inches; jet angle, 90°.
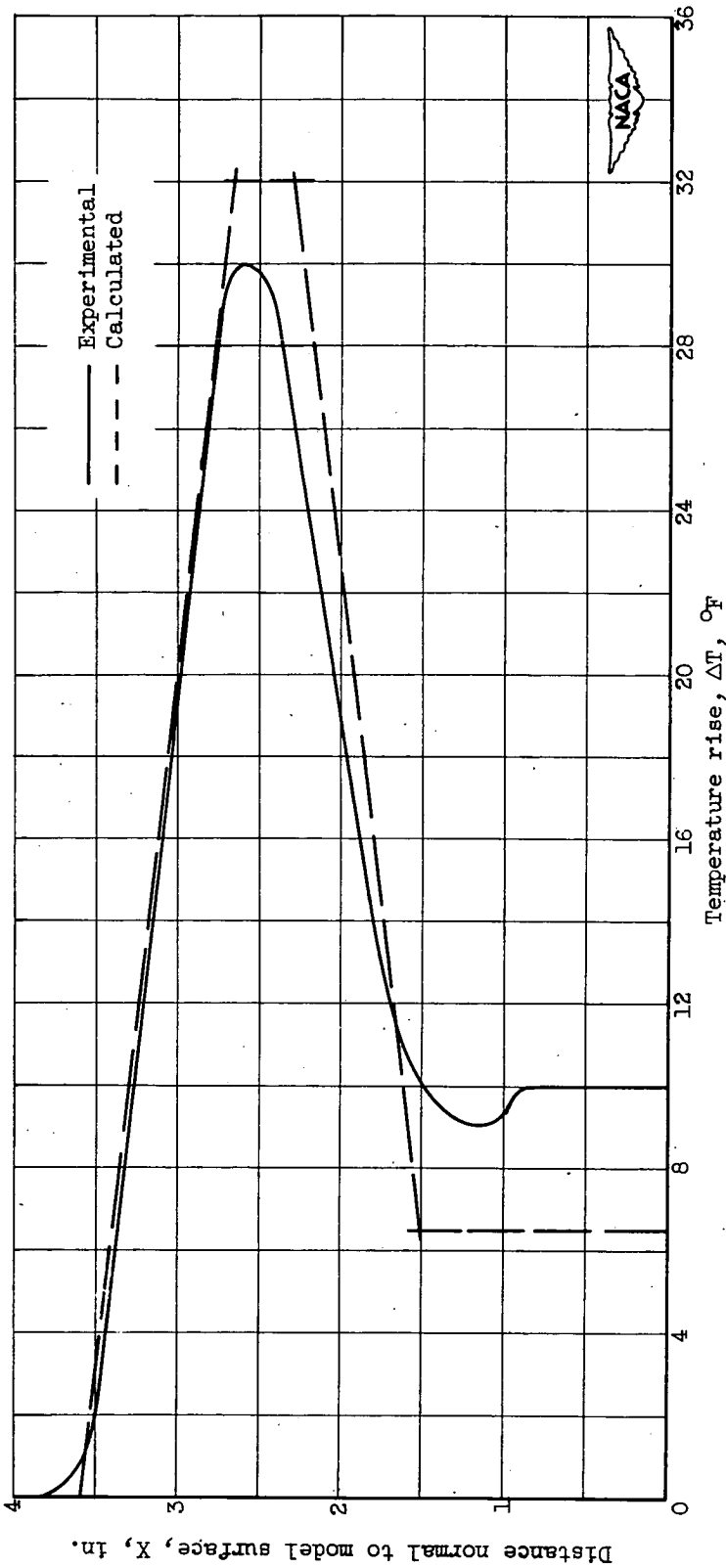
Figure 30. – Comparison of calculated and experimental temperature profiles.
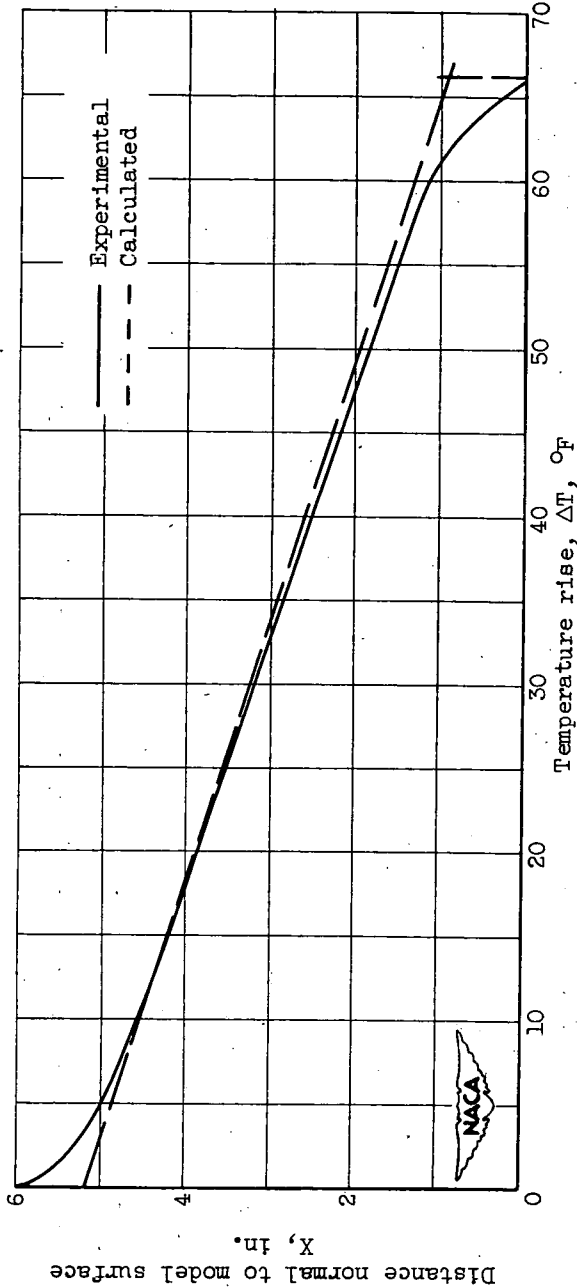
(b) Orifice diameter, 0.625 inch; jet total temperature, 860° R; jet pressure ratio, 2.2; free-stream velocity, 235 feet per second; rake position, 18.0 inches; jet angle, 60°.

Figure 30. - Continued.　Comparison of calculated and experimental temperature profiles.
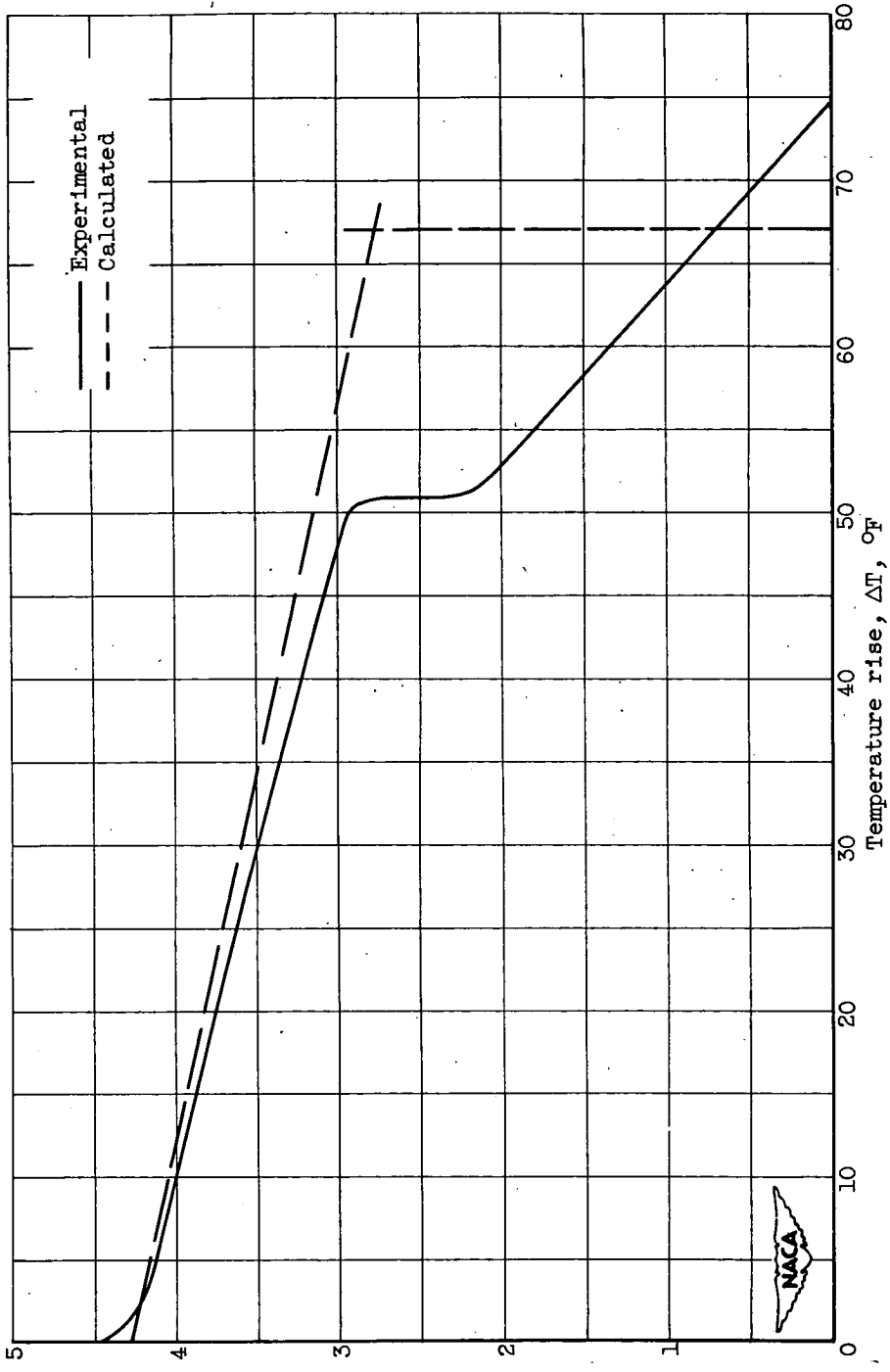
(c) Orifice diameter, 0.625 inch; jet total temperature, 8860° R; jet pressure ratio, 2.53; free-stream velocity, 235 feet per second; rake position, 6.47 inches; jet angle, 60°.

Figure 30. - Continued. Comparison of calculated and experimental temperature profiles.

(d) Orifice diameter, 0.375 inch; jet total temperature, 860° R; jet pressure ratio, 3.02; free-stream velocity, 235 feet per second; rake position, 6.47 inches; jet angle, 45°.

Figure 30. - Concluded. Comparison of calculated and experimental temperature profiles.
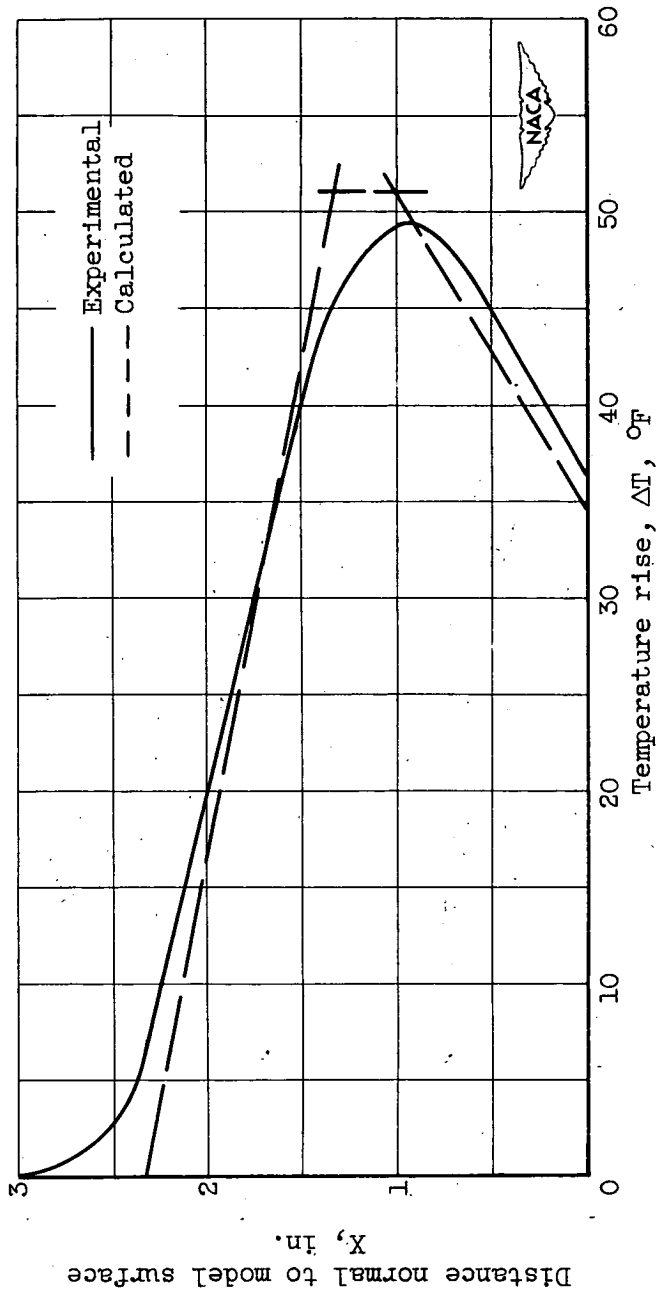
Figure 31. - Comparison of calculated and experimental temperature profiles for jet operating at pressure ratio below choking. Jet pressure ratio, 1.36; orifice diameter, 0.625 inch; jet total temperature, 840° R; free-stream velocity, 400 feet per second; rake position, 6.47 inches; jet angle, 90°.
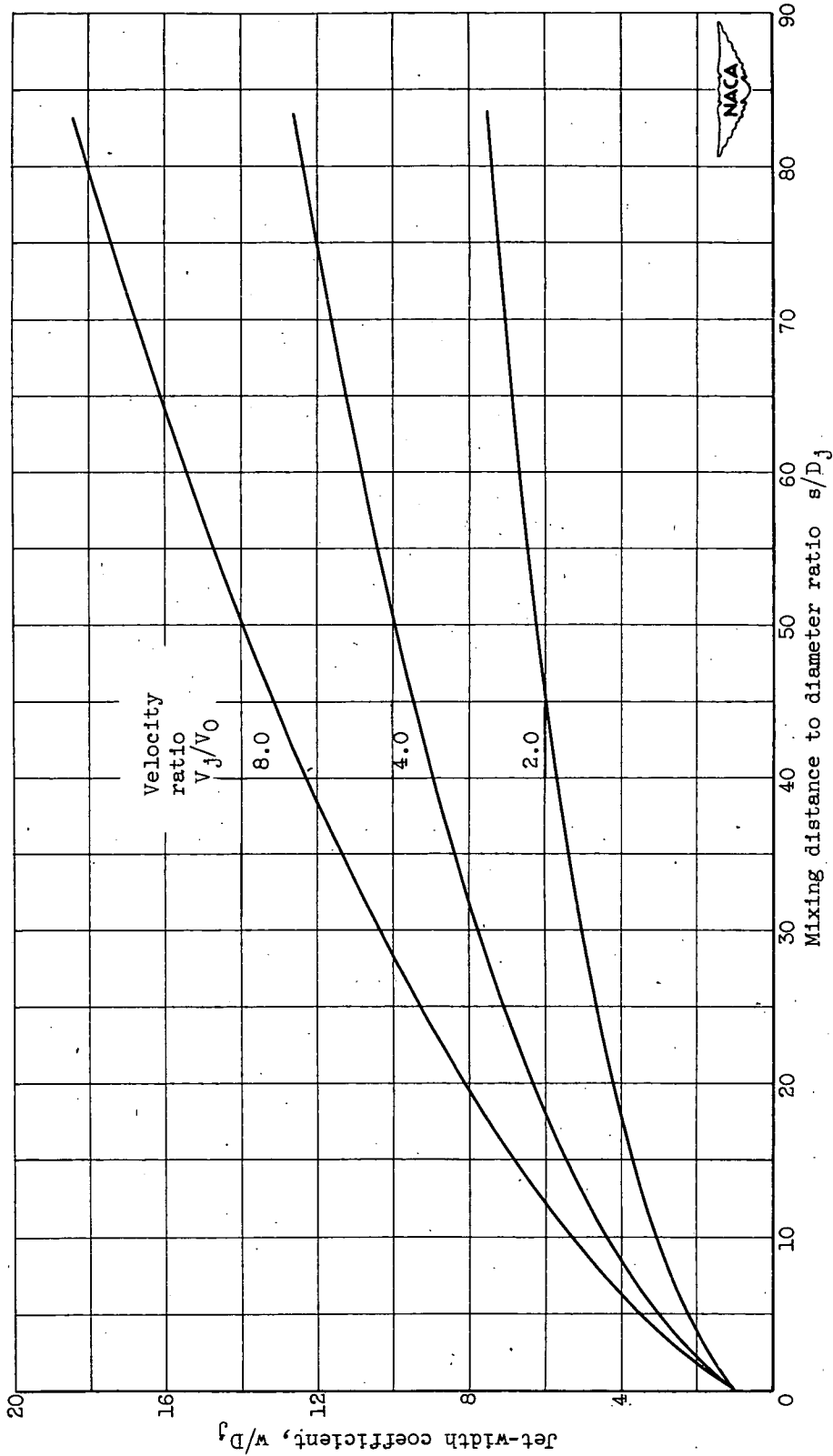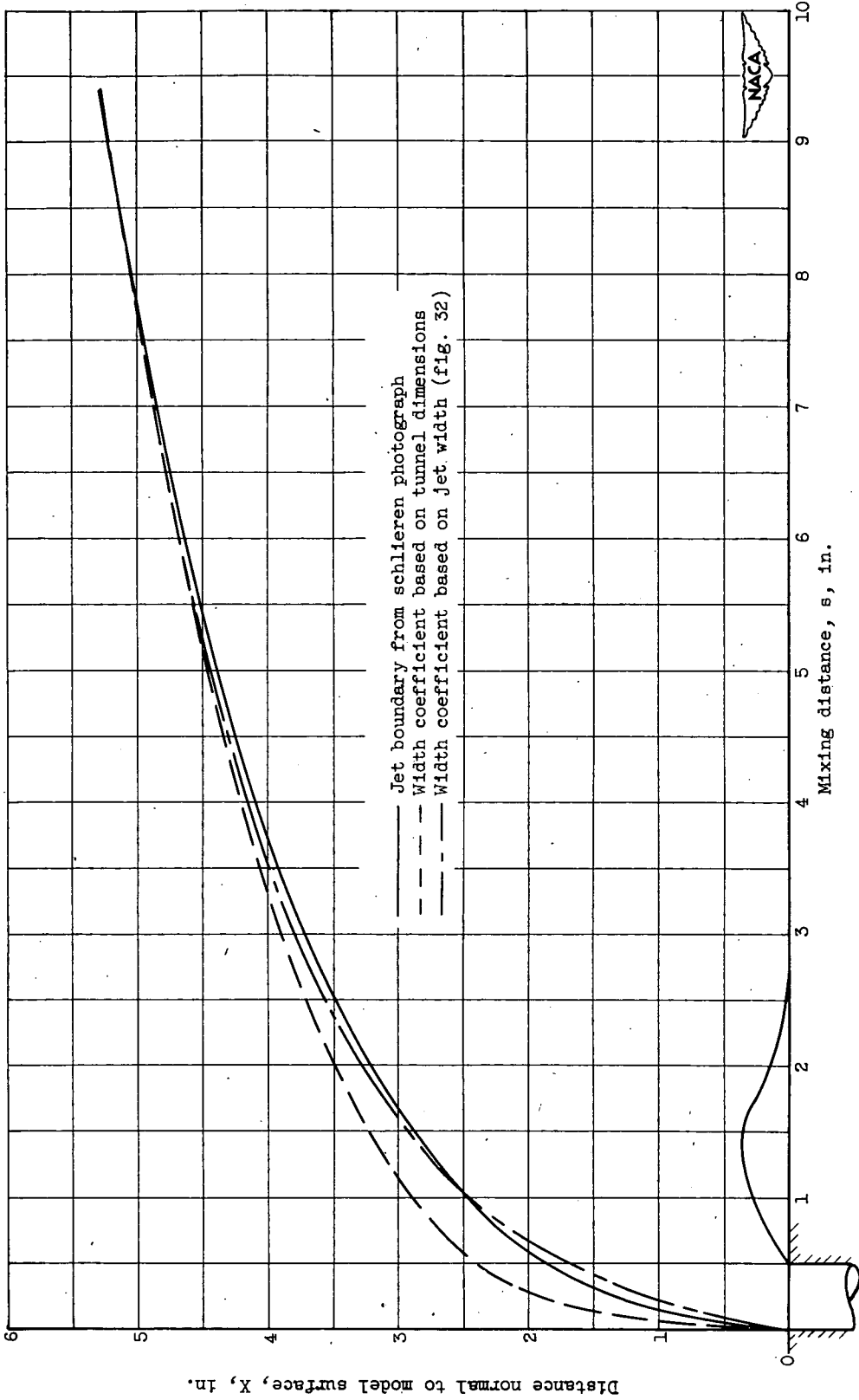
Figure 32. - Variation of jet-width coefficient w/D_j with mixing distance to diameter ratio for three velocity ratios.

Distance normal to model surface, X, in.

Mixing distance, s, in.

——— Jet boundary from schlieren photograph
– – – Width coefficient based on tunnel dimensions
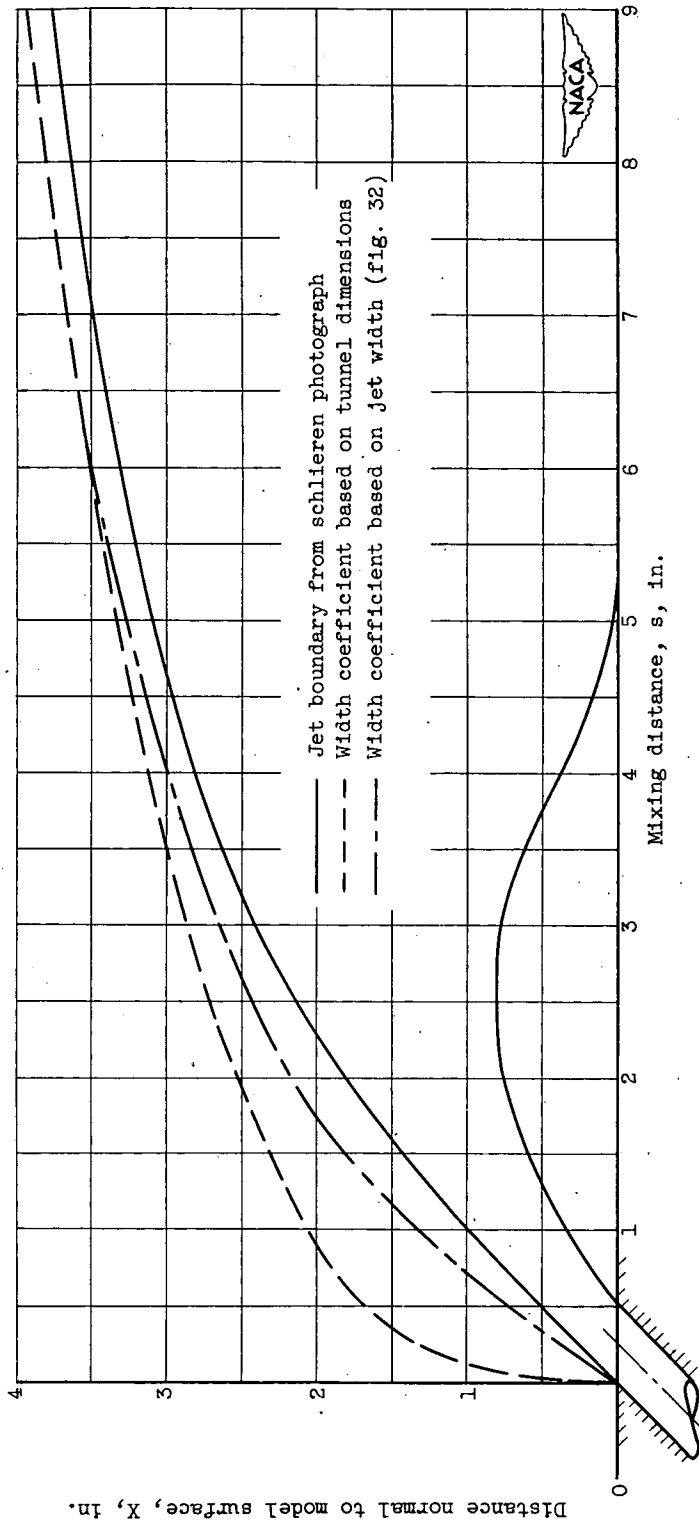— – — Width coefficient based on jet width (fig. 32)

(a) Orifice diameter, 0.500 inch; jet total temperature, 660° R; jet pressure ratio, 3.33; free-stream velocity, 375 feet per second; jet angle, 90°.

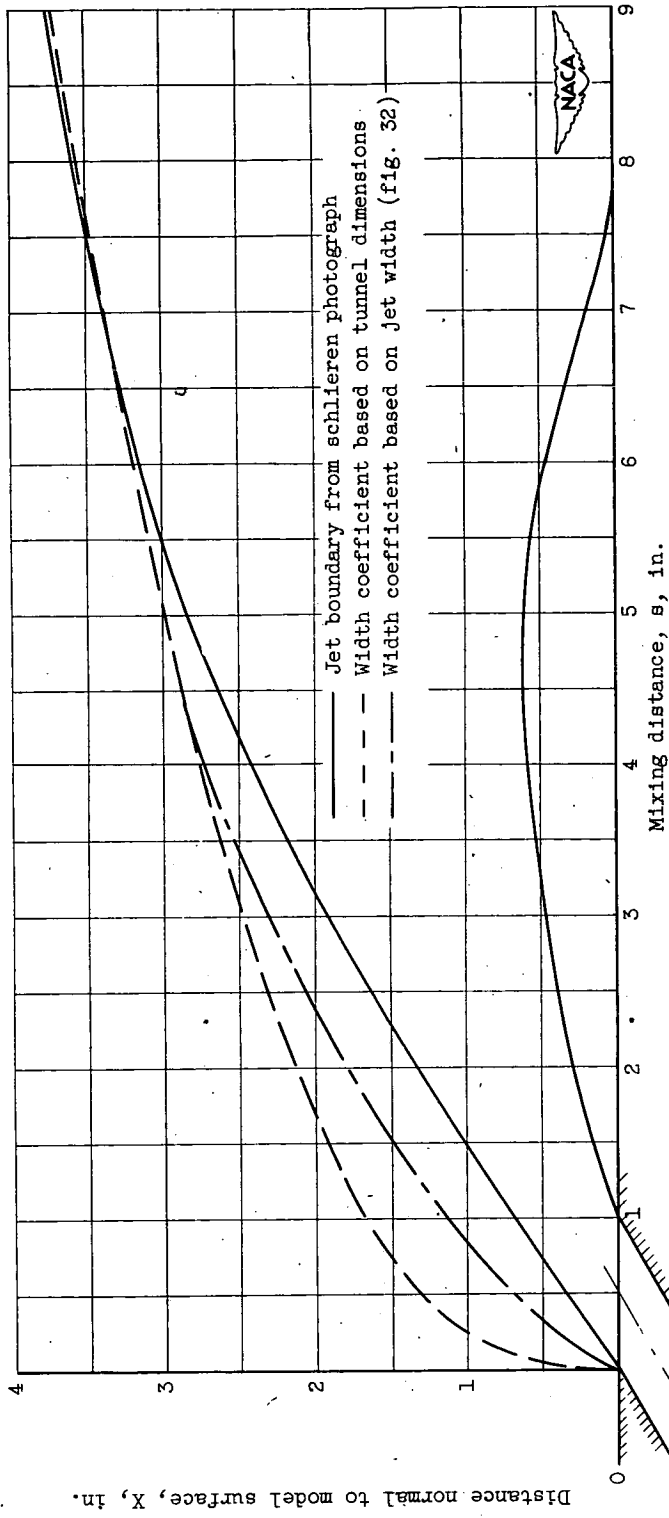Figure 33. - Comparison of calculated and experimental jet boundaries.
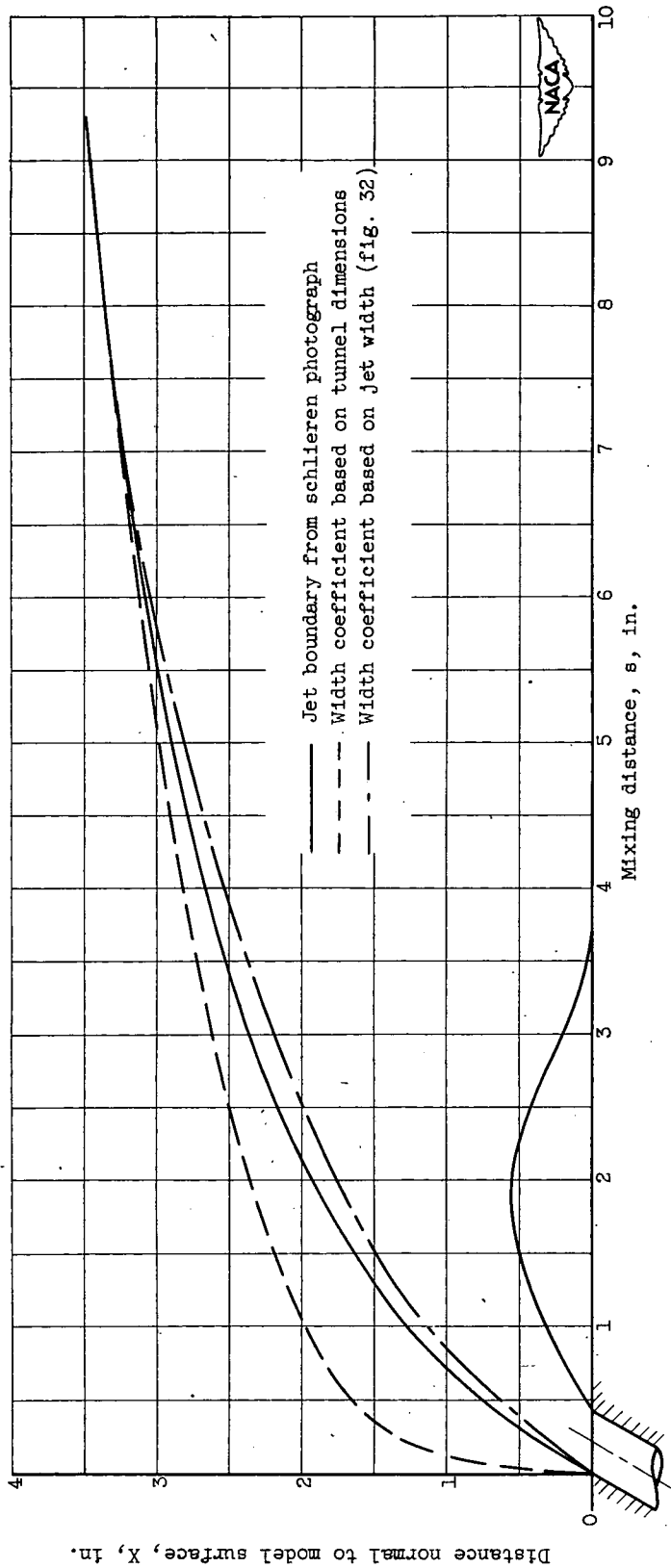
(b) Orifice diameter, 0.375 inch; jet total temperature, 860° R; jet pressure ratio, 3.15; free-stream velocity, 395 feet per second; jet angle, 60°.

Figure 33. - Continued. Comparison of calculated and experimental jet boundaries.

(c) Orifice diameter, 0.375 inch; jet total temperature, 860° R; jet pressure ratio, 2.86; free-stream velocity, 232 feet per second; jet angle, 45°.

Figure 33. - Continued. Comparison of calculated and experimental jet boundaries.

(d) Orifice diameter, 0.500 inch; jet total temperature, 660° R; jet pressure ratio, 2.93; free-stream velocity, 235 feet per second; jet angle, 30°.

Figure 33. - Concluded. Comparison of calculated and experimental jet boundaries.